Inorganic Chemistry

Article

pubs.acs.org/IC

Functionalization Reactions Characteristic of a Robust Bicyclic Diphosphane Framework

Daniel Tofan,[†] Manuel Temprado,*[,‡] Subhojit Majumdar,[§] Carl D. Hoff,*[,§] and Christopher C. Cummins*[,†]

[†]Department of Chemistry, Massachusetts Institute of Technology, 77 Massachusetts Avenue, Cambridge, Massachusetts 02139, United States

[‡]Department of Physical Chemistry, Universidad de Alcalá, Ctra. Madrid-Barcelona Km. 33,600, Madrid 28871, Spain

[§]Department of Chemistry, University of Miami, 1301 Memorial Drive, Coral Gables, Florida 33021, United States

Supporting Information

ABSTRACT: The 3,4,8,9-tetramethyl-1,6-diphospha-bicyclo-[4.4.0]deca-3,8-diene ($P_2(C_6H_{10})_2$) framework containing a P−P bond has allowed for an unprecedented selectivity toward functionalization of a single phosphorus lone pair with reference to acyclic diphosphane molecules. Functionalization at the second phosphorus atom was found to proceed at a significantly slower rate, thus opening the pathway for obtaining mixed functional groups for a pair of P−P bonded λ^5-phosphorus atoms. Reactivity with the chalcogen-atom donors MesCNO (Mes = 2,4,6-$C_6H_2Me_3$) and $SSbPh_3$ has allowed for the selective synthesis of the diphosphane chalcogenides $OP_2(C_6H_{10})_2$ (87%), $O_2P_2(C_6H_{10})_2$ (94%), $SP_2(C_6H_{10})_2$ (56%), and $S_2P_2(C_6H_{10})_2$ (87%). Computational studies indicate that the oxygen-atom transfer reactions involve penta-coordinated phosphorus intermediates that have four-membered {PONC} cycles. The P−E bond dissociation enthalpies in $EP_2(C_6H_{10})_2$ were measured via calorimetric studies to be 134.7 ± 2.1 kcal/mol for P−O, and 93 ± 3 kcal/mol for P−S, respectively, in good agreement with the computed values. Additional reactivity with breaking of the P−P bond and formation of diphosphinate $O_3P_2(C_6H_{10})_2$ was only observed to occur upon heating of dimethylsulfoxide solutions of the precursor. Reactivity of diphosphane $P_2(C_6H_{10})_2$ with azides allowed the isolation of monoiminophosphoranes $(RN)P_2(C_6H_{10})_2$(R = Mes, CPh_3, $SiMe_3$), and treatment with additional $MesN_3$ yielded symmetric and unsymmetric diiminodiphosphoranes $(RN)(MesN)$-$P_2(C_6H_{10})_2$ (91% for R = Mes). Metalation reactions with the bulky diiminodiphosphorane ligand $(MesN)_2P_2(C_6H_{10})_2$ (nppn) allowed for the isolation and characterization of (nppn)Mo(η^3-C_3H_5)Cl(CO)$_2$ (91%), (nppn)$NiCl_2$ (76%), and [(nppn)Ni(η^3-2-C_3H_4Me)][OTf] showing that these ligands provide an attractive preorganized binding pocket for both late and early transition metals.

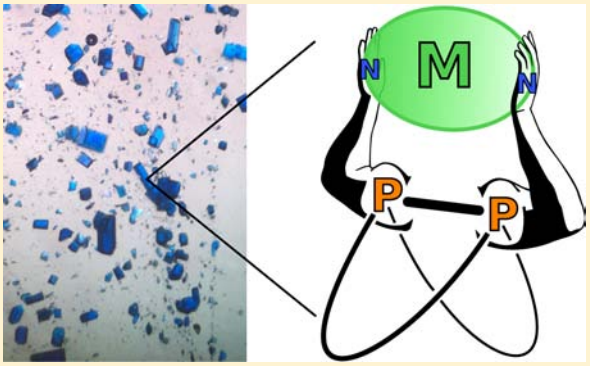

INTRODUCTION

Since the first report on the synthesis of multicyclic tetraorganodiphosphane molecules by effective sequential Diels−Alder addition of two 1,3-diene molecules to P_2,[1] our group has uncovered a synthetically useful, one-step synthesis of bicyclic diphosphanes from the co-photolysis of P_4 (white phosphorus) and 1,3-dienes.[2] Following the discovery of a streamlined route to synthesize the 3,4,8,9-tetramethyl-1,6-diphosphabicyclo[4.4.0]deca-3,8-diene[3] ($P_2(C_6H_{10})_2$, **1**, Figure 1), we have investigated the advantages that stem from having a fixed dihedral angle between the two phosphorus lone pairs with respect to the formation of bimetallic complexes.[4] With the present work, we report our investigations on functionalization reactions at the two phosphorus lone pairs of diphosphane **1** together with characterization data for the diphosphorane (bis-λ^5-phosphane) products.

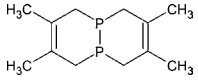

Figure 1. 3,4,8,9-Tetramethyl-1,6-diphosphabicyclo[4.4.0]deca-3,8-diene (diphosphane **1**).

Although the literature of metal complexes with phosphorane ligands is extensive,[5] research on complexes of diphosphoranes containing P−P bonds ($R_2P(E)-P(E)R_2$) has been limited almost exclusively to diphosphane disulfides (E = S, Chart 1). In addition, while phosphine sulfides have been reported as ligands for precursors in homogeneous catalysis,[6,7] no such reports exist for using diphosphorane ligands with an intact P−P bond. These observations are quite surprising since such ligands would chelate and presumably form very stable five-

Received: April 27, 2013
Published: July 10, 2013

   dx.doi.org/10.1021/ic401052a | *Inorg. Chem.* 2013, 52, 8851−8864

Chart 1. Metal-Binding Modes Available to Diphosphorane Ligands with P−P Bonds

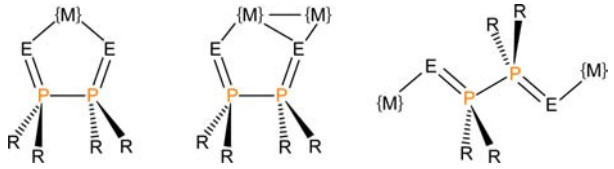

membered $\{ME_2P_2\}$ metallacycles, which ought to exhibit enhanced stability toward decomposition compared to monodentate phosphorane ligands.

The majority of the reported diphosphane disulfide complexes involve mono- and divalent late transition metals,[8] and a few involve metals from groups 6 and 7.[9] Spectroscopic evidence has also been presented for a diphosphane dioxide chelating to iron(II) and zinc(II) centers (E = O, R = Ph),[10] for a dioxide bridging two molybdenum(VI) centers (E = O, R = *n*-C_3H_7),[11] and a diselenide chelating to a nickel(II) center (E = Se, R = Ph).[12] Several binding modes can be envisioned in these complexes (Chart 1), yet unambiguous molecular structures have been determined only for a few selected examples. The first structure of a binuclear complex with chelating diphosphane disulfide ligands (Chart 1, center) was reported by Cotton et al. for copper(I) (R = Me).[13] The structures of mononuclear complexes (Chart 1, left) have only been reported in four cases: copper(I) (R = Me), silver(I) (R = Me), rhodium(I) (R = Et), and palladium(II) (PR_2 = $P(NEt_2)$(cyclohexyl)).[14]

A candidate explanation for the scarcity of examples wherein diphosphoranes have been used for metal chelation is that they are typically acyclic and thus allow for free rotation about the P−P bond, rotation which in turn may lead to rearrangement and formation of bridges between two metal centers instead of robust metallacycles (Chart 1, right). For example, it was shown that in the presence of copper(II), $Me_2P(S)-P(S)Me_2$ yields a bimetallic complex with chelating ligands in a Gauche conformation (Chart 1, center),[13] as well as a polymer with disulfide ligands bridging between metal centers in an anti configuration (Chart 1, right).[15] Cyclic diphosphoranes are much less common, but employing such frameworks would prevent rotation about the P−P bond and lock the two sulfur atoms in an eclipsed conformation. However, functionalization of monocyclic diphosphanes has only allowed for the formation of *trans*-disulfides, which are not suitable for metal chelation.[16] *Cis*-diphosphane disulfides (Chart 2) have only been achieved

Chart 2. Diphosphane Dichalcogenides with a Locked *cis* Configuration

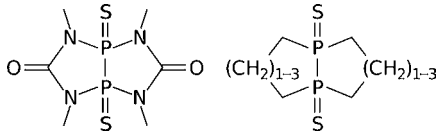

by functionalizing bicyclic diphosphanes.[17] Still, *cis* bicycles are required for this conversion, yet there is only a relatively limited number of reports of diphosphanes with such a locked *cis* configuration.[18]

Additional groups near the chelation pocket may prevent some of the degradation pathways that are accessible to diphosphane dichalcogenide complexes, such as aggregation into multimetallic complexes (Chart 1, center). In addition, they could allow for increased solubility in nonpolar solvents, and thus potentially expand on the applications demonstrated for less soluble diphosphane dichalcogenides. Iminophosphoranes are a good model for this behavior because the imine group can provide steric bulk in the immediate vicinity of the metal center. In contrast to α-diimines, which have been widely used as ligands for homogeneous catalysis,[19,20] diiminodiphosphorane analogues containing a P−P bond have not been readily accessible, and only a few have been reported.[21,22] Several cyclic diiminodiphosphoranes have been prepared from iminophosphanes of the type RP═NMes* (R = Me, ^{t}Bu, Ph; Mes* = 2,4,6-^{t}Bu$_3$C$_6$H$_2$) via P−P coupling reactions,[21] but they exhibit *trans* imino substituents and are not suitable for metal chelation. There is a single example of direct diiminodiphosphorane synthesis from acyclic diphosphanes (R_2P-PR_2, R = Me, Et, *n*-Pr, *n*-Bu) via treatment with an inorganic azide (Me_3SiN_3).[22] Nonetheless, the reactivity of these diiminodiphosphoranes has only been investigated in relation to P−N bond cleavage.[23]

Use of a bicyclic framework such as the diphosphane **1** ought to allow the synthesis of diphosphoranes with substituents locked in a *cis* configuration. We report here the synthesis of diphosphane dichalcogenides and diiminodiphosphoranes with a conserved bicyclic framework and with substituents that are confined to an eclipsed conformation. In addition, we demonstrate that the *cis*-diimine derivatives offer an attractive, preorganized binding pocket that accommodates transition-metal centers.

RESULTS AND DISCUSSION

Oxygen-Atom Transfer Reactions. Although methods for preparing diphosphane monoxides are available, there are very few examples that illustrate their synthesis directly from the parent diphosphane. For example, the oxidation of commercially accessible P_2Ph_4 to $Ph_2P-P(O)Ph_2$ has not been achieved selectively.[24] Only for cyclic diphosphanes with bulky substituents has the oxidation been achieved selectively with H_2O_2 or $(Me_3Si)_2O_2$.[25] Mono-oxidation of a 1,1′-biphosphole was also achieved with $(Me_3Si)_2O_2$ over a period of 7 days.[26] We uncovered a new method for achieving a single oxidation of a diphosphane selectively by employing the oxygen-atom transfer (OAT) reagent mesitylnitrile-*N*-oxide (MesCNO; Mes = 2,4,6-$C_6H_2Me_3$).

In the presence of MesCNO, the diphosphane **1** acts as an oxygen-atom acceptor at the phosphorus lone pairs. Dropwise treatment of **1** with 1 equiv of MesCNO at room temperature led to the selective formation of the diphosphane monoxide $OP_2(C_6H_{10})_2$ (**1**-O) within minutes (Scheme 1). The product precipitated out of diethyl ether solutions as a white powder and was isolated in 87% yield. In the solid state, monoxide **1**-O (Figure 2) exhibits a slight diminution of the P−P distance to 2.2034(5) Å as compared to a 2.2218(5) Å distance found in diphosphane **1**,[2] consistent with an increased positive charge on the phosphorus(IV) atom. Natural Bond Orbital (NBO) analysis[27] on **1**-O did indeed reveal a partial charge of +1.52 on the phosphorus(IV) atom, while the charge on the phosphorus(II) atom at +0.43 remains relatively unchanged from that in diphosphane **1** (Table 3). The pure product appears to be indefinitely stable in solution at room temperature and it does not decompose even upon prolonged heating (120 °C, toluene), as isomerization to a diphosphinite via O-atom insertion into the P−P bond was predicted through

dx.doi.org/10.1021/ic401052a | *Inorg. Chem.* 2013, 52, 8851−8864

Scheme 1. Oxidation of the Diphosphane 1 with 1 and 2 equiv of MesCNO

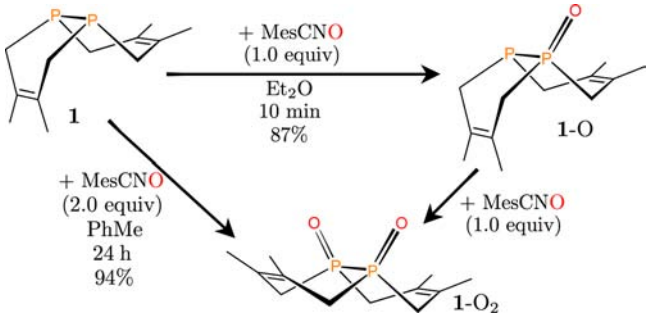

density functional theory (DFT) methods to be unfavorable by 6.7 kcal/mol.

The enthalpy of the OAT reaction of MesCNO with diphosphane **1** was measured experimentally at −82.4 ± 2.0 kcal/mol by reaction calorimetry (eq 1), which corresponds to a P−O bond dissociation enthalpy (BDE) in **1**-O of 134.7 ± 2.1 kcal/mol (BDE of N−O in MesCNO is 52.3 ± 0.7 kcal/mol[28]). The P−O BDE is between those for trialkyl and triaryl phosphine oxides, as comparable measurements for phosphines such as $OPMe_3$, $OPCy_3$, and $OPPh_3$ yielded 138.5, 137.6, and 132.2 kcal/mol, respectively.[28]

$$\mathbf{1} + \text{MesCNO} \xrightarrow{\Delta H = -82.4 \pm 2.0\ \text{kcal/mol}} \mathbf{1}\text{-O} + \text{MesCN} \qquad (1)$$

DFT computations were employed to corroborate the experimental BDE value, and to understand the mechanism of the oxidation reaction. The reaction enthalpy was computed to be −78.7 kcal/mol, corresponding to a P−O BDE of 131.0 kcal/mol, in good agreement with the experimental value (eq 1). The simplified model framework 1,6-diphospha-bicyclo-[4.4.0]deca-3,8-diene (**1**′, $P_2(C_4H_6)_2$, with H replacing the Me groups in **1**) and 2,6-$Me_2C_6H_3CNO$ were used for investigating the mechanism of the OAT. A productive pathway was found to involve a two-step process with an intermediate containing a four-membered {PONC} ring similar to those observed for the oxidation of PR_3 phosphines (Figure 3).[28] This mechanism is similar to that of the Staudinger reaction between phosphines and organic azides,[29] and it involves little change in the P−P distance and an activation barrier $\Delta H^{\ddagger}$ of 10.0 kcal/mol.

If the monoxide **1**-O is allowed to form in a solvent in which it is soluble, it undergoes further oxidation with MesCNO to form the symmetric dioxide $O_2P_2(C_6H_{10})_2$ (**1**-O_2, Scheme 1). This second OAT is much slower and required stirring a toluene solution of diphosphane **1** and 2 equiv of MesCNO for 24 h at room temperature to generate the dioxide **1**-O_2 for a

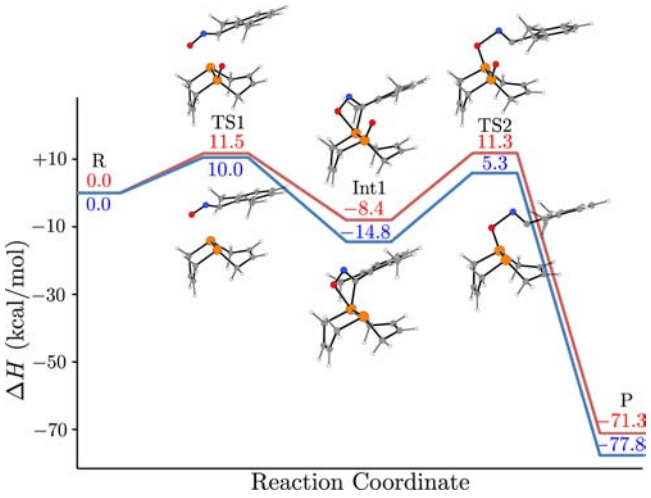

Figure 3. Relative enthalpies for the OAT reactions from 2,6-$Me_2C_6H_3CNO$ to **1**′ (bottom, blue) and to **1**′-O (top, red), respectively. R corresponds to a molecule of 2,6-$Me_2C_6H_3CNO$ and either **1**′ or **1**′-O, while P corresponds to a molecule of 2,6-$Me_2C_6H_3CN$ and either **1**′-O or **1**′-O_2 set at infinite distances.

94% isolated yield. In solution, the dioxide was stable even after 12 h in refluxing benzene and exhibited a C_{2v} molecular symmetry (^{1}H NMR). In the solid state, the dioxide **1**-O_2 is rigorously C_s-symmetric along the {OPPO} plane (Figure 2) and adopts an *exo-exo* configuration which is in contrast to the *exo-endo* conformations adopted by the monoxide **1**-O and unfunctionalized bicyclic diphosphanes.[2]

The enthalpy of this second OAT from MesCNO to the diphosphane monoxide **1**-O could not be measured experimentally because of the slow reaction rate and the low solubility of the product. It was computed, however, to be −72.5 kcal/mol (eq 2). This corresponds to a P−O BDE of 124.8 kcal/mol, which is 6.2 kcal/mol lower than the computed P−O BDE in **1**-O. The mechanism of the formation of dioxide **1**-O_2 is similar to that observed for **1**-O, as it involves a four-membered ring intermediate and an activation barrier $\Delta H^{\ddagger}$ of 11.5 kcal/mol (Figure 3).

$$\mathbf{1}\text{-O} + \text{MesCNO} \xrightarrow{\Delta H = -72.5\ \text{kcal/mol}} \mathbf{1}\text{-O}_2 + \text{MesCN} \qquad (2)$$

A subtle, yet important difference was observed between the activation enthalpies of the first OAT step of **1**′ with 2,6-$Me_2C_6H_3CNO$ and that of the second step. The slight increase in activation enthalpy from 10.0 to 11.5 kcal/mol corresponds to a 12-fold decrease in reaction rate at room temperature from the first to the second OAT. When removing the *ortho* groups (using PhCNO), the activation enthalpies change to 10.2 and

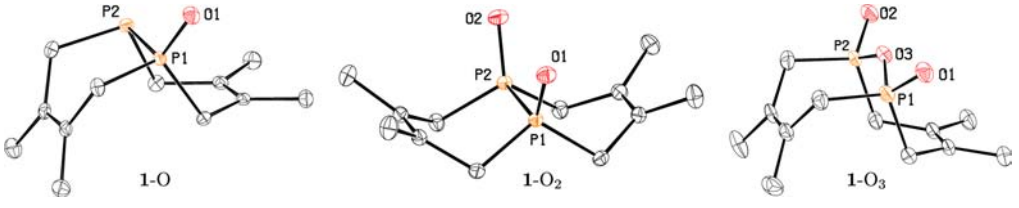

Figure 2. Solid-state structures of the diphosphane oxides with ellipsoids at the 50% probability level and hydrogen atoms omitted for clarity. Selected interatomic distances [Å] and angles [deg] for monoxide **1**-O (left): P1−P2 2.2034(5), P1−O1 1.4959(10), O1−P1−P2 114.65(5); for dioxide **1**-O_2 (center): P1−P2 2.2185(7), P1−O1 1.4934(16), P2−O2 1.4935(15), O1−P1−P2 113.88(6), O2−P2−P1 113.72(7), O1−P1−P2−O2 0.0(0); for trioxide **1**-O_3 (right): P1−P2 2.9257(13), P1−O1 1.513(3), P2−O2 1.4792(18), P1−O3 1.5972(16), P2−O3 1.609(2), O1−P1−O3 109.10(17), O2−P2−O3 109.67(9), P1−O3−P2 131.73(10), O1−P1−P2−O2 1.0(3).

dx.doi.org/10.1021/ic401052a | *Inorg. Chem.* 2013, 52, 8851−8864

10.8 kcal/mol, respectively. This implies that steric repulsions of *ortho*-methyl groups with the already installed chalcogen atom are responsible for the selectivity toward the singly functionalized **1**-O. Previously reported selective monooxidations of diphosphanes[25,26] are likely to involve some type of steric repulsions, but here however, these are a result of the bicyclic nature of the diphosphane framework **1** that prevents the oxo group from rotating away from the *ortho* groups of MesCNO.

No additional reactivity of dioxide **1**-O_2 with excess MesCNO could be observed, as oxidation to the P−P bond-cleaved diphosphinate $O_3P_2(C_6H_{10})_2$ (**1**-O_3) was only achieved with boiling Me_2SO solutions of **1**-O_2. Exposing solutions of diphosphane **1** at room temperature to air however, led to the formation of a mixture of all three oxides. The air stability of various phosphines has been correlated to the energy level of the singly occupied molecular orbital (SOMO) of their radical cation.[30] We computed that the radicals $[\mathbf{1}]^{\bullet+}$ and $[\mathbf{1}\text{-O}]^{\bullet+}$ have SOMOs localized on the phosphorus atoms at −10.0 and −10.2 eV, respectively. These values are close to the −10 eV threshold above which phosphines have been predicted to be air stable.[30] A very slow air oxidation was observed for diphosphane **1**, consistent with the proposed threshold.

Crystals of the trioxide **1**-O_3 in an *exo-endo* configuration (Figure 2) were obtained by aging a solution of **1** in air. Notably, a minor disorder component consisting of the *exo-endo* conformer of dioxide **1**-O_2 was observed in this crystal (Supporting Information, Figure S.2), thus provides experimental evidence for a very low energy difference between the *exo-exo* and *exo-endo* isomers of derivatives of diphosphane **1**. Indeed, DFT calculations revealed that for diphosphane **1′**, the *exo-endo* isomer surmounts a barrier of only 5.9 kcal/mol with a reaction enthalpy of just 2.5 kcal/mol for converting into the *exo-exo* isomer (Figure 4). Solution ^{1}H NMR spectra of **1** show

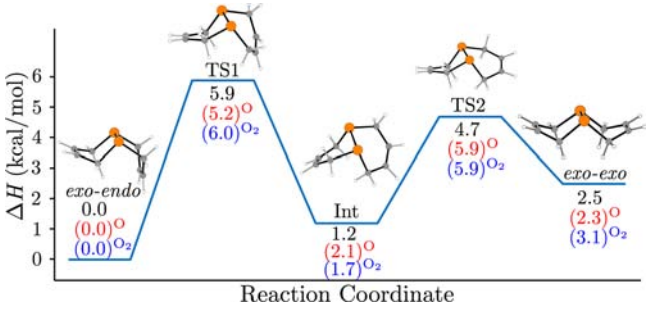

Figure 4. Relative enthalpies for the interconversion of diphosphane **1′** (numbers in black) between the *endo-exo* and the *exo-exo* conformers (eq 3). Very similar values were observed for the conversions of the monoxide **1′**-O (in red) and dioxide **1′**-O_2 (in blue) conformers.

no changes at temperatures as low as −90 °C, and with such a low calculated barrier, no changes are anticipated above −160 °C.[31] Similar values were computed for the interconversion of conformers of oxides **1′**-O and **1′**-O_2 (Figure 4). This suggests that the *exo-exo* configuration observed for the dioxide **1**-O_2 in the solid state may be solely a result of favorable crystal packing interactions. In addition, such small barriers are consistent with fast exchange between conformers in solution (eq 3), which results in fast equilibration of the ^{1}H NMR environments on the bicyclic backbone of derivatives of diphosphane **1** and an apparent σ-symmetry plane containing the P−P bond.

$$\textit{exo-endo} \rightleftharpoons \textit{exo-exo} \rightleftharpoons \textit{endo-exo} \qquad (3)$$

Sulfur-Atom Transfer (SAT) Reactions. Using appropriate chalcogen transfer reagents, heavier analogues of the oxides were also obtained. Treatment of diphosphane **1** with 1 equiv of $SSbPh_3$ in benzene led to the formation of the monosulfide $SP_2(C_6H_{10})_2$ (**1**-S) as a precipitate, which could be isolated pure in 56% yield. The enthalpy of the reaction was also measured via calorimetry at −25.7 ± 1.0 kcal/mol (eq 4), which corresponds to a P−S BDE of 93 ± 3 kcal/mol (BDE of S−Sb in $SSbPh_3$ is 67 ± 3 kcal/mol[32]). The P−S BDE is slightly larger than that measured for $SPPh_3$ (88 kcal/mol), but slightly smaller than that for $SPMe_3$ (94 kcal/mol).[32] DFT computations predicted the P−S BDE to be 90 kcal/mol, corroborating well the measured experimental value.

$$\mathbf{1} + SSbPh_3 \xrightarrow{\Delta H=-25.7\pm1.0\ \text{kcal/mol}} \mathbf{1}\text{-S} + SbPh_3 \qquad (4)$$

Addition of a second equivalent of $SSbPh_3$ to solutions of **1** led to rapid generation of the disulfide $S_2P_2(C_6H_{10})_2$ (**1**-S_2, Scheme 2). Likely because of the less sterically demanding

Scheme 2. Synthesis of the Disulfide 1-S_2

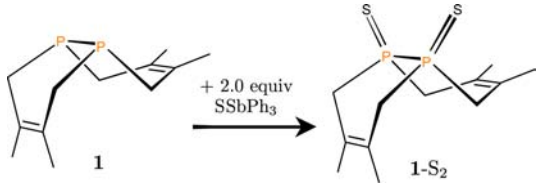

nature of $SSbPh_3$ as compared with MesCNO, the second SAT step occurs at a comparable rate with the formation of **1**-S, thus allowing for calorimetric measurements (eq 5). The reaction enthalpy is only slightly higher compared to the first sulfurization, implying a second BDE of 94 ± 3 kcal/mol. The disulfide **1**-S_2 was isolated in 87% yield following treatment of **1** with 2 equiv of $SSbPh_3$ for 2 h. Unlike the dioxide **1**-O_2, the disulfide **1**-S_2 adopts an *endo-exo* configuration in the solid state (Figure 5) with a small S−P−P−S angle of about 2°. The

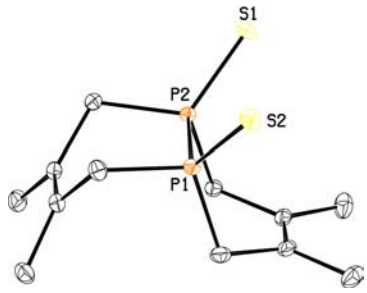

Figure 5. Solid-state structure of the diphosphane disulfide **1**-S_2 with ellipsoids at the 50% probability level and hydrogen atoms omitted for clarity. Selected interatomic distances [Å] and angles [deg]: P1−P2 2.2192(4), P1−S1 1.9489(4), P2−S2 1.9495(4), S1−P1−P2 114.170(15), S2−P2−P1 114.823(16), S1−P1−P2−S2 1.96(2).

monosulfide and disulfide exhibit similar NMR spectroscopic features to those observed for the monoxide and the dioxide, respectively (Table 1).

$$\mathbf{1}\text{-S} + SSbPh_3 \xrightarrow{\Delta H=-25.0\pm1.1\ \text{kcal/mol}} \mathbf{1}\text{-}S_2 + SbPh_3 \qquad (5)$$

Nitrene-Group Transfer (NGT) Reactions. Similar to other dichalcogenides that contain a P−P bond, the dichalcogenides **1**-E_2 provide well-poised chelating pockets

dx.doi.org/10.1021/ic401052a | Inorg. Chem. 2013, 52, 8851−8864

Table 1. Spectroscopic and Structural Parameters of Phosphorane Derivatives of 1

compound	$\delta_{\lambda^5 P}$[a]	$\delta_{\lambda^{3/5} P}$[a]	$^1J_{P-P}$[b]	P−P[c]	E−P−P−E[d]
1-O	+75.9	−87.4	217	2.2034(5)	
1-S	+62.0	−62.0	280		
1-NMes	+30.7	−97.9	274		
1-$NCPh_3$	+36.9	−98.9	296		
1-O_2	+11.5			2.2185(7)	0
1-S_2	+20.4			2.2192(4)	1.96(2)
1-$(NMes)_2$	−35.7			2.2398(5)	5.57(10)
1-$(NCPh_3)$(NMes)	−30.9	−33.0	93	2.2805(7)	10.95(11)

[a] δ_{31_P} [ppm] in C_6D_6 (for **1**:[2] —53.6 ppm). [b] Experimental $^1J_{P-P}$ [Hz] (for η^1-**1**:[4] 344 Hz). [c] Interatomic distances [Å] (for **1**:[2] 2.2218(5) Å). [d] Dihedral angles [deg].

Scheme 3. Synthesis of Mono- and Diiminodiphosphoranes 1-NR and 1-(NR)(NMes)

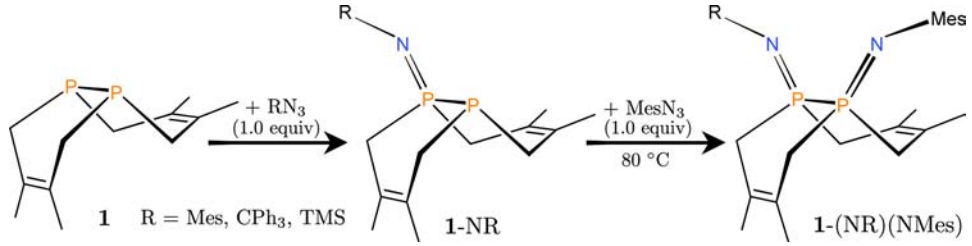

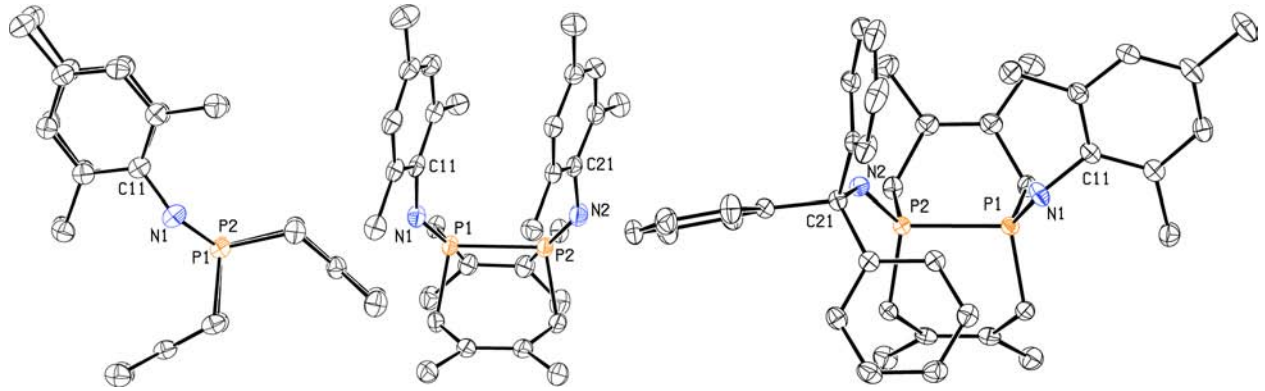

Figure 6. Solid-state structure of the symmetric and the unsymmetric diiminodiphosphoranes **1**-$(NMes)_2$ (left and center) and **1**-$(NCPh_3)$(NMes) (right) with ellipsoids at the 50% probability level and hydrogen atoms omitted for clarity. Selected interatomic distances [Å] and angles [deg] for **1**-$(NMes)_2$: P1−P2 2.2398(5), P1−N1 1.5531(13), P2−N2 1.5459(14), N1−P1−P2 120.61(5), N2−P2−P1 120.70(6), C11−N1−P1 140.53(12), C21−N2−P2 140.72(12), N1−P1−P2−N2 5.57(10); and for **1**-$(NCPh_3)$(NMes): P1−P2 2.2805(7), P1−N1 1.5561(15), P2−N2 1.5504(16), N1−P1−P2 124.25(6), N2−P2−P1 114.39(6), C21−N2−P2 134.51(14), C31−N1−P1 131.48(13), N1−P1−P2−N2 10.95(11).

for accommodating various metal centers. However, because of their bicyclic nature, they exhibit a rigid structure with small E−P−P−E dihedral angles. Despite this attractive feature, the low solubility of these molecules in low-dielectric organic media has been an impediment in studying them as partners in metalation reactions. In searching for more soluble variants, we decided to target the iminophosphorane derivatives. The Staudinger reaction of phosphines with organic azides has been shown to have a similar mechanism[29] to the one proposed between phosphines and MesCNO.[28] As a result, it was deemed logical to similarly investigate the reactions of diphosphane **1** with RN_3 azide molecules.

Treatment with $MesN_3$ led to a vigorous evolution of dinitrogen coupled with the formation of the monoiminophosphorane $(MesN)P_2(C_6H_{10})_2$ (**1**-NMes). At room temperature, the diphosphane **1** reacted to completion with 1 equiv of $MesN_3$ within 30 min (Scheme 3). Further conversion was observed when additional $MesN_3$ was present but, as with MesCNO, this second step was significantly slower than the initial formation of **1**-NMes. Upon heating to 80 °C, the consumption of monoiminophosphorane **1**-NMes became fast and was coupled with vigorous evolution of dinitrogen. Refluxing the diphosphane **1** in benzene in the presence of 2 equiv of $MesN_3$ led to the clean formation of diiminodiphosphorane $(MesN)_2P_2(C_6H_{10})_2$ (**1**-$(NMes)_2$, nppn) after 12 h. Upon cooling, crystals of analytically pure diiminodiphosphorane formed, giving a 91% isolated yield.

The iminophosphoranes **1**-NMes and **1**-$(NMes)_2$ present similar features as observed for the chalcogenides **1**-E and **1**-E_2, respectively. In solution, they exhibit C_s and C_{2v} molecular symmetries, respectively (^{1}H NMR), but in the solid state, the diiminodiphosphorane **1**-$(NMes)_2$ exhibits a low symmetry with distinct environments for each of its ten methyl groups (Figure 6). Steric crowding from the mesityl groups led to a

dx.doi.org/10.1021/ic401052a | Inorg. Chem. 2013, 52, 8851−8864

notable increase in P−P distance and N−P−P−N dihedral angle compared to the dichalcogenides.

Treatment of diphosphane **1** with more electron-rich azides led to qualitatively slower reaction rates. In the particular case of trityl azide, heating the reaction mixture in benzene at 70 °C for 9 h was needed for clean, complete conversion to the monoiminophosphorane $(Ph_3CN)P_2(C_6H_{10})_2$ (**1**-$NCPh_3$). No further reactivity was observed upon continued heating at 90 °C in the presence of excess Ph_3CN_3. However, in the presence of $MesN_3$, this monoiminophosphorane is converted to the unsymmetric monomesityl, monotrityl diiminodiphosphorane $(MesN)(Ph_3CN)P_2(C_6H_{10})_2$ (**1**-$(NCPh_3)(NMes)$). In the solid state, the P−P interatomic distance is slightly elongated from that in **1**-$(NMes)_2$, while the N−P−P−N dihedral angle is above 10° (Figure 6). Inorganic azides react even more slowly with **1**, as the reactions with Ph_3SiN_3 or Me_3SiN_3 required additional heating after 9 h at 70 °C to complete the conversion to the corresponding monoiminophosphorane products. No reaction was observed between diphosphane **1** and Ph_3SnN_3 even after 36 h of heating at 90 °C.

Examples of monoiminophosphoranes with P−P bonds are plentiful in the literature, yet there has been only one report describing the synthesis of iminophosphoranes directly from their parent R_2P-PR_2 diphosphanes (R = Me, Et, *n*-Pr, *n*-Bu).[22] The reaction of acyclic diphosphanes with Me_3SiN_3 necessitated heating of the neat reagents to 100 °C to produce mixtures of both monoimino- and diimino-functionalized products. Control over selectivity could only be achieved by varying the number of azide equivalents used, and isolation of iminophosphorane-phosphanes and diiminodiphosphoranes necessitated separation via distillation.[22] As reported above, use of diphosphane **1**, however, allowed for complete selectivity control without requiring tedious purification. In fact, except for the aryl azide $MesN_3$, no azide underwent a second Staudinger reaction at the remaining proximal phosphorus atom under the tested conditions.

Such selectivity for monofunctionalization of diphosphane **1** allows facile access to **1**-E molecules. These are potential ligands for binding metal centers in either an κ^1 fashion or a κ^2P,E mode with the formation of four-membered {MPPE} metallacycles. The potential of these monophosphoranes as ligands has been investigated in silico for the κ^1P binding mode. Using $Ni(CO)_3$ as a metal fragment (Figure 7), the Tolman

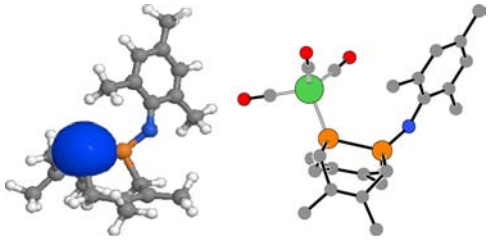

Figure 7. NBO analysis of **1**-NMes shows a well-defined phosphorus lone pair (left, in blue) which can be used for metal binding such as in $(OC)_3Ni((\mathbf{1}\text{-NMes})\text{-}\kappa^1P)$ (right, DFT-optimized structure).

electronic parameter can be extracted from the totally symmetric stretch of the $Ni(CO)_3$ unit (Table 2).[33] The contribution χ_i from the λ^5-phosphorus substituent $(P(=E)R_2)$ was computed to be 7 to 10 cm^{-1} higher than in the unfunctionalized diphosphane **1**. For comparison, this substituent contribution increases by around 15 cm^{-1} upon going from a methyl to a fluorine substituent.[33] This is in contrast to the minimal change in the NBO s-orbital character (Table 3), indicating a significant inductive effect with little change in geometry at the phosphorus atom.

Table 2. Tolman Electronic Parameters for Mono-Functionalized 1-E Derivatives Compared to PMe_3, PPh_3, and PF_3

compound	$\nu_{CO}(A_1)(cm^{-1})$	$\Delta\nu_{PMe_3}$ $(cm^{-1})^a$	$\chi_{P(E)R2}$ $(cm^{-1})^b$
1	2042.9	−1.7	4.0
1′	2045.6	1.0	6.7
1-O	2051.9	7.3	13.0
1-S	2052.9	8.3	14.0
1-Se	2052.2	7.6	13.3
1-NMes	2050.3	5.7	11.4
PMe_3[c]	2044.6(2064.1)	0	2.6(2.6)
PPh_3[c]	2046.3(2068.9)	1.7	3.3(4.3)
PF_3[c]	2090.1(2110.8)	45.5	17.9(18.2)

[a] $\Delta\nu_{PMe_3} = \nu_{CO}(\mathbf{1}\text{-E}) - \nu_{CO}(PMe_3)$. [b] $\chi_{P(E)R_2} = \nu_{CO}(A_1)_E - 2036.5 - 2 \times \chi_{iBu}$, where **1**-E have been approximated to $(^iBu)_2P-P(E)(^iBu)_2$ (χ_{iBu} = 1.2 cm^{-1}).[33] [c] Experimental values are shown inside parentheses.[33]

Table 3. NBO Analysis for Mono-Functionalized 1-E Derivatives Compared to PMe_3, PPh_3, and PF_3

		natural charge on		
compound	s-orbital character of P lone-pair (%)	λ^3-P	λ^5-P	E
1	59.8	0.46		
1′	60.8	0.45		
1-O	61.3	0.43	1.52	−1.00
1-S	61.3	0.49	0.94	−0.54
1-Se	61.2	0.50	0.84	−0.47
1-NMes	61.5	0.44	1.40	−0.96
PMe_3	54.4	0.70		
PPh_3	49.4	0.75		
PF_3	75.2	1.59		

Metal Complexes of Diiminodiphosphoranes. Molecules containing two iminophosphorane groups such as $CH_x(Ph_2P{=}NR)_2$ have been used as ligands in many metal-catalyzed reactions.[34] In contrast, complexes that incorporate diiminodiphosphorane ligands and that contain a P−P bond have not yet been reported. This is quite surprising when considering that the latter class of ligands could prove to be valuable counterparts to the α-diimines that have been employed as ligands for a wide range of applications in transition-metal catalysis.[19,20] The bicyclic diiminodiphosphoranes reported here are superficially similar to α-diimine ligands and offer a restricted rotation about the P−P bond. The diiminodiphosphorane **1**-$(NMes)_2$ (nppn) framework was considered to constitute an attractive bidentate ligand for applications in transition-metal chemistry, and metalation reactions were accordingly carried out with both early and late transition-metal sources.

Molybdenum(II) diimine complexes have been shown to be good catalyst precursors for epoxidation of alkenes,[35] leading us to target diiminodiphosphorane analogues. Treatment of molybdenum(II) source $MoCl(CO)_2(\eta^3\text{-}C_3H_5)(NCMe)_2$[36] with nppn in dichloromethane (Scheme 4), allowed for the isolation of the $(nppn)MoCl(CO)_2(\eta^3\text{-}C_3H_5)$ complex (**2**) as a

dx.doi.org/10.1021/ic401052a | *Inorg. Chem.* 2013, 52, 8851−8864

Scheme 4. Synthesis of Molybdenum(II) Complex (nppn)MoCl(CO)$_2$(η^3-C$_3$H$_5$)

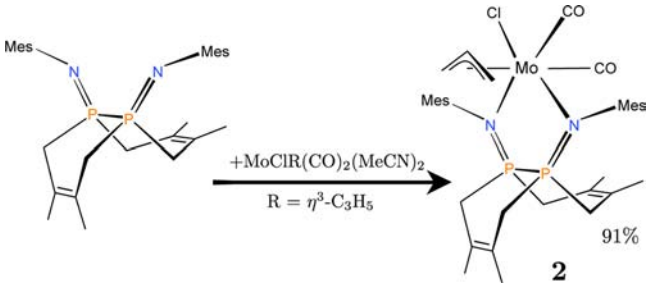

pale yellow powder in 91% yield. NMR spectroscopy revealed broad features indicative of a low-symmetry complex engaging in a slow exchange process, and two broad ^{31}P NMR resonances near +6 ppm ($^1J_{P-P}$ = 180 Hz) that imply two different substituents *trans* to the nitrogen atoms of the chelating nppn ligand. Indeed, the solid-state structure obtained for the complex **2** reveals a *pseudo*-octahedral geometry around molybdenum, with a carbonyl and an allyl group occupying the positions *trans* to the nppn chelate (Figure 8). The N−Mo−N bite angle of 81.54(7)° is similar to the angle in molybdenum(II) α-diimine complexes.[35] The metallacycle exhibits an envelope conformation, with almost coplanar P−N bonds (N−P−P−N: 1.28(11)°; P−P−N−Mo: 21.51(12)° and 25.11(12)°). The longer Mo−N bond observed *trans* to the CO ligand is consistent with the strong structural *trans* influence of CO.[37] Compared to the free nppn, chelation led to a slight elongation of the P−N distances by about 0.05 Å, coupled with significant shortening of the P−P distance to 2.1525(9) Å. This distance is almost 0.1 Å shorter than in free nppn and is the shortest P−P distance of all the compounds reported herein, this being consistent with the electron-withdrawing effect of a Lewis-acidic metal center.

Nickel(II) α-diimine complexes are desirable synthetic targets as many have been shown to exhibit high activities toward olefin polymerization.[20] We targeted analogous diiminodiphosphorane complexes and isolated the deep-turquoise, paramagnetic nickel(II) complex (nppn)NiCl$_2$ (**3**) in 76% yield from the treatment of nppn with the NiCl$_2$(dme) precursor (Scheme 5, dme = 1,2-dimethoxyethane). The solid-state structure of the paramagnetic complex **3** reveals a *pseudo*-tetrahedral geometry around the nickel(II) center (Figure 8). As with complex **2**, the metallacycle exhibits an envelope conformation with almost coplanar P−N bonds (N−P−P−N: 4.91(14)°; P−P−N−Ni: 16.84(14)° and 24.47(14)°) and contains almost equal Ni−N distances, with a shortened P−P but elongated P−N distances when compared to free nppn. A square-planar nickel(II) complex was also obtained by treating half of an equivalent of the [NiCl(η^3-2-C$_3$H$_4$Me)]$_2$ dimer in dichloromethane with AgOTf in the presence of nppn (Scheme 5, OTf = CF$_3$SO$_3$). The [(nppn)Ni(η^3-2-C$_3$H$_4$Me)][OTf] product (**4**) was crystallized from the filtrate as a golden powder, in 59% yield. The nickel complex **4** exhibits diamagnetism characteristic of square-planar nickel(II) centers with a low-spin d^8 electronic configuration. Although it shows a sharp ^{31}P NMR singlet resonance (+25 ppm), the complex manifests two distinct ^{1}H NMR environments for the *ortho*-mesityl groups and two for the methyl groups on the bicyclic backbone. This *pseudo*-C_s symmetry (with a σ plane through Ni and the middle of the P−P bond) is indicative of a crowded, rigid environment around the metal center, where the mesityl groups are locked on one side of the {NiN$_2$} plane.

CONCLUDING REMARKS

The synthesis of diphosphoranes was achieved directly from diphosphane **1** by taking advantage of the rigidity inherent to its bicyclic nature. The pronounced stability of **1** toward P−P bond breaking reactions has allowed for selective functionalization reactions which are not available for acyclic diphosphanes. Reactivity of **1** with the OAT reagent MesCNO has been investigated in detail using computational and calorimetric techniques. Sequential OAT reactions allowed for clean formation of a monoxide and a dioxide; further oxidation involving the cleavage of the P−P bond is much slower.

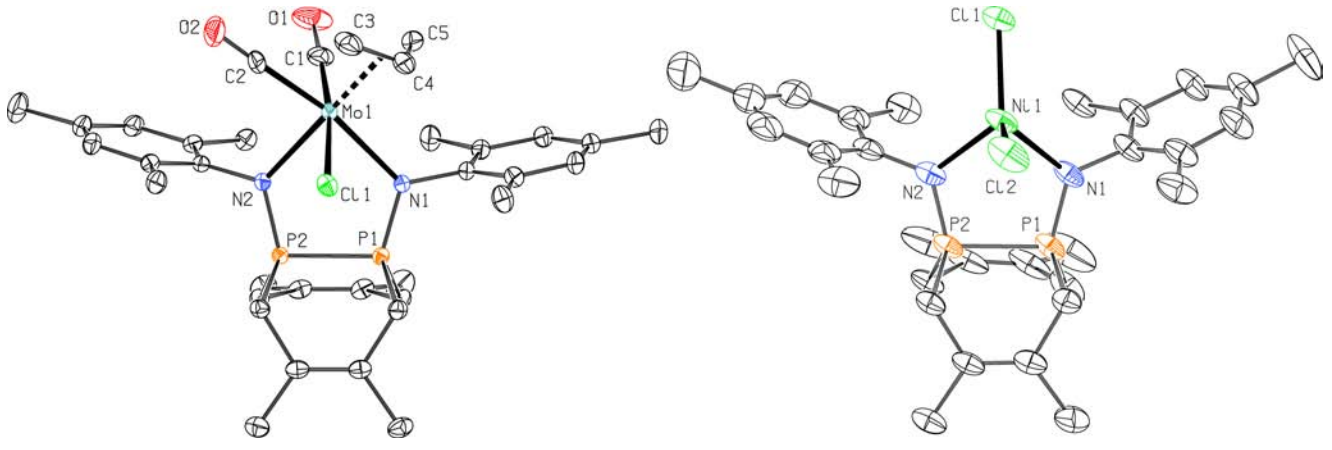

Figure 8. Solid-state structures of the molybdenum(II) **2** and nickel(II) **3** nppn complexes with ellipsoids at the 50% probability level; solvent molecules and hydrogen atoms were omitted for clarity. Selected interatomic distances [Å] and angles [deg] for **2**: P1−P2 2.1525(9), Mo1−N1 2.317(2), Mo1−N2 2.244(2), Mo1−C1 1.918(3), Mo1−C2 1.949(3), Mo1−Cl1 2.6213(7), P1−N1 1.600(2), P2−N2 1.605(2), N2−Mo1−N1 81.54(7), P1−N1−Mo1 117.46(10), P2−N2−Mo1 120.17(11), N1−P1−P2 105.98(8), N2−P2−P1 103.91(8), C4−Mo1−N2 165.37(9), C2−Mo1−N1 169.23(10), C1−Mo1−Cl1 173.12(10), N1−P1−P2−N2 1.28(11), P2−P1−N1−Mo 21.51(12), P1−P2−N2−Mo 25.11(12); for **3**: P1−P2 2.1676(12), Ni1−N2 2.011(3), Ni1−N1 2.019(3), P1−N1 1.586(3), P2−N2 1.585(3), N2−Ni1−N1 93.88(11), P1−N1−Ni1 113.02(14), P2−N2−Ni1 114.53(16), N1−P1−P2 104.16(12), N2−P2−P1 104.10(11), Cl1−Ni1−Cl2 122.58(4), N1−P1−P2−N2 4.91(14), P2−P1−N1−Ni 16.84(14), P1−P2−N2−Ni 24.47(14).

dx.doi.org/10.1021/ic401052a | Inorg. Chem. 2013, 52, 8851−8864

Scheme 5. Syntheses of Nickel(II) Complexes (nppn)$NiCl_2$ and [(nppn)Ni(η^3-2-C_3H_4Me)][OTf]

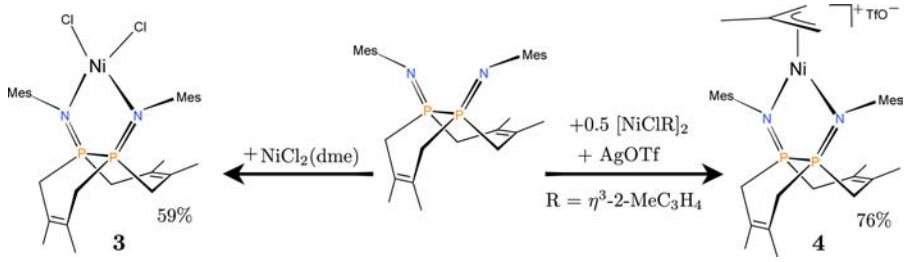

Phosphine sulfides were isolated from treatment of diphosphane **1** with $SSbPh_3$, while treatment of **1** with organic azides led to formation of mono- and diiminodiphosphoranes via sequential Staudinger reactions. Functionalization at the second phosphorus atom is significantly slower than for the first one, permitting the installation of mixed functional groups on the phosphorus atoms. Metalation reactions with diiminodiphosphoranes have shown that these ligands provide an attractive preorganized binding pocket for both late and early transition metals. All these chemical transformations have demonstrated that a stable and versatile platform is provided by the diphosphane backbone **1**.

EXPERIMENTAL DETAILS

General Synthetic Details. Unless otherwise stated, all manipulations were performed in a Vacuum Atmospheres model MO-40 M glovebox under an inert atmosphere of purified N_2. Solvents were obtained anhydrous and oxygen-free by sparging with N_2 and purifying using a Glass Contours Solvent Purification System (SG Water). Deuterated solvents were purchased from Cambridge Isotope Laboratories, degassed, and stored over molecular sieves prior to use. All glassware was oven-dried at temperatures greater than 170 °C prior to use. Celite 435 (EM Science) was dried by heating above 200 °C under a dynamic vacuum for at least 48 h prior to use, while alumina (activated, basic, Brockman I) was dried similarly for at least 7 days prior to use. NMR spectra were obtained on Varian Mercury 300, Varian Inova 500, or Bruker Avance 400 instruments equipped with Oxford Instruments superconducting magnets, and were referenced to the appropriate solvent resonances.[38] ^{31}P NMR spectra were referenced externally to 85% H_3PO_4 (0 ppm). The following abbreviations were used to explain the multiplicities: s = singlet, d = doublet, t = triplet, q = quartet, m = multiplet, br = broad, v = virtual multiplet. Elemental analyses were performed by Midwest Microlab LLC, Indianapolis, IN. White phosphorus was acquired from Thermphos International. Diphosphane **1**,[4] MesCNO,[39] $MesN_3$,[40] Ph_3EN_3,[41] and $[Mo(CO)_2Cl(\eta^3\text{-}C_3H_5)(NCMe)_2]$[36] were prepared and isolated according to literature protocols, while the other reagents were acquired from commercial sources.

Synthesis of Monoxide $OP_2(C_6H_{10})_2$ (1-O). A solution of MesCNO (71 mg, 0.44 mmol, 1.0 equiv) in Et_2O (3 mL) was added dropwise, over a period of 5 min, to a solution of **1** (100 mg, 0.44 mmol, 1.0 equiv) in Et_2O (6 mL). White precipitate started forming halfway through the addition; the mixture was stirred for another 5 min after the addition was complete. The final mixture was diluted with pentane (10 mL), and the white solids were collected on a fritted glass filter, washed with pentane (10 mL), and dried under reduced pressure. A white powder consisting of pure $OP_2(C_6H_{10})_2$ was obtained (93 mg, 0.38 mmol, 87% yield). ^1H NMR (C_6D_6, 20 °C, 400 MHz) δ: 2.37 (dd, $^2J_{HP}$ = 18.2 Hz, $^2J_{HH}$ = 15.0 Hz, 2 H, OPCH*H*), 2.14 (pst, 12.2 Hz, 2 H, OPC*H*H), 2.02 (psq, 14.4 Hz, 2 H, PCH*H*), 1.76 (dd, $^2J_{HP}$ = 22.7 Hz, $^2J_{HH}$ = 14.0 Hz, 2 H, PC*H*H), 1.54 (s, 6 H, PCH_2CCH_3), 1.39 (s, 3 H, $OPCH_2CCH_3$), 1.37 (s, 3 H, $OPCH_2CCH_3$) ppm; assignments were made based on the ^1H-^1H COSY NMR spectrum (Supporting Information, Figure S.1). $^{13}C\{^1H\}$ NMR (C_6D_6, 20 °C, 100.6 MHz) δ: 127.1 (dd, $^2J_{CP}$ = 12 Hz, $^3J_{CP}$ = 1.5 Hz, $OPCH_2CH_0$), 124.7 (dd, $^2J_{CP}$ = 9 Hz, $^3J_{CP}$ = 4 Hz, PCH_2CH_0), 36.7 (d, $^1J_{CP}$ = 41.8 Hz, $OPCH_2$), 28.9 (dd, $^1J_{CP}$ = 26.5 Hz, $^2J_{CP}$ = 4.5 Hz, PCH_2), 21.4 (d, $^3J_{CP}$ = 1.0 Hz, CH_3), 21.2 (d, $^3J_{CP}$ = 3.2 Hz, CH_3) ppm. $^{31}P\{^1H\}$ NMR (C_6D_6, 20 °C, 161.9 MHz) δ: +75.9 (d, $^1J_{PP}$ = 217 Hz, 1 P, O*P*P), −87.4 (d, 1 P, OP*P*) ppm. ^{31}P NMR ($CDCl_3$, 20 °C, 121.5 MHz) δ: +82.1 (d), −84.9 (d). Elemental analysis [%] found (and calcd. for $C_{12}H_{20}P_2O$): C 59.37 (59.50); H 8.17 (8.32); N none (0.00).

Synthesis of Dioxide $O_2P_2(C_6H_{10})_2$ (1-O_2). A solution of MesCNO (123 mg, 0.76 mmol, 2.0 equiv) in toluene (2 mL) was added dropwise over 3 min to a solution of **1** (86 mg, 0.38 mmol, 1.0 equiv) in toluene (3 mL). The mixture became cloudy within minutes, but was allowed to stir for 24 h. After diluting with Et_2O (5 mL), the white precipitate was collected on a fritted glass filter, washed with Et_2O (10 mL), and dried under reduced pressure. A white powder consisting of pure $O_2P_2(C_6H_{10})_2$ (92 mg, 0.36 mmol, 94% yield) was collected. ^1H NMR (DMSO-d_6, 20 °C, 400 MHz) δ: 3.03 (dd, $^2J_{HH}$ = 14.6 Hz, $^2J_{HP}$ = 7.6 Hz, 4 H, OPCH*H*), 2.68 (d, 4 H, OPC*H*H), 1.74 (s, 12 H, CH_3) ppm. $^{13}C\{^1H\}$ NMR (DMSO-d_6, 20 °C, 100.6 MHz) δ: 123.8 (s, CH_0), 34.8 (vt, $^{12}J_{CP}$ = 27.7 Hz, CH_2), 21.4 (s, CH_3) ppm. $^{31}P\{^1H\}$ NMR (DMSO-d_6, 20 °C, 121.5 MHz) δ: +16.2 (s) ppm. $^{31}P\{^1H\}$ NMR (C_6D_6, 20 °C, 121.5 MHz) δ: +11.5 (s) ppm. ^{31}P NMR ($CDCl_3$, 20 °C, 121.5 MHz) δ: +14.1 (s) ppm. Elemental analysis [%] found (and calcd. for $C_{12}H_{20}P_2O_2$): C 56.40 (55.81); H 8.59 (7.81); N none (0.00).

Generation of Trioxide $O_3P_2(C_6H_{10})_2$ (1-O_3). A solution of monoxide **1**-O (10 mg, 0.76 mmol, 2.0 equiv) in DMSO-d_6 (1 mL) inside an NMR tube was heated via a heat-gun for 5 min until the solvent started boiling, after which, NMR spectroscopic analysis showed the presence of only trioxide **1**-O_3. ^1H NMR ($CDCl_3$, 20 °C, 400 MHz) δ: 2.93 (br s, 8 H, CH_2), 1.87 (s, 12 H, CH_3) ppm. ^1H NMR (DMSO-d_6, 20 °C, 400 MHz) δ: 2.85 (vbr s, 8 H, CH_2), 1.77 (s, 12 H, CH_3) ppm. ^{13}C NMR ($CDCl_3$, 20 °C, 100.6 MHz) δ: 125.5 (s, CH_0), 38.8 (vt, $^{12}J_{CP}$ = 19.5 Hz, CH_2), 22.3 (s, CH_3) ppm. $^{31}P\{^1H\}$ NMR ($CDCl_3$, 20 °C, 162 MHz) δ: +22.1 (s) ppm. $^{31}P\{^1H\}$ NMR (DMSO-d_6, 20 °C, 162 MHz) δ: +12 (s) ppm.

Synthesis of Monosulfide $SP_2(C_6H_{10})_2$ (1-S). To a solution of **1** (94 mg, 0.41 mmol, 1.0 equiv) in Et_2O (5 mL) a suspension of $SSbPh_3$ (160 mg, 0.41 mmol, 1.0 equiv) in Et_2O (5 mL) was added dropwise. After 1 h of vigorous stirring, the suspension was filtered and washed with Et_2O (10 mL), and the white powder was dried under reduced pressure to yield **1**-S (60 mg, 0.23 mmol, 56%). ^1H NMR (C_6D_6, 20 °C, 400 MHz) δ: 2.35 (d, $^2J_{HP}$ = 13.5 Hz, 2 H, SPCH*H*), 2.05 (m, 2 H, SPC*H*H), 1.89 (m, 2 H, PCH*H*), 1.75 (m, 2 H, PC*H*H), 1.57 (s, 6 H, PCH_2CCH_3), 1.38 (s, 3 H, $SPCH_2CCH_3$), 1.36 (s, 3 H, $SPCH_2CCH_3$) ppm. $^{13}C\{^1H\}$ NMR (C_6D_6, 20 °C, 100.6 MHz) δ: 128.8, 125.7, 39.9, 31.5, 22.9, 22.7 ppm. $^{31}P\{^1H\}$ NMR (C_6D_6, 20 °C, 121.5 MHz) δ: +62.0 (d, $^1J_{PP}$ = 280 Hz, 1 P, S*P*P), −62.0 (d, 1 P, SP*P*) ppm. ^{31}P NMR ($CDCl_3$, 20 °C, 162 MHz) δ: +62.6 (d, $^1J_{PP}$ = 277 Hz, 1 P, S*P*P), −59.1 (d, 1 P, SP*P*) ppm. Elemental analysis [%] found (and calcd. for $C_{12}H_{20}P_2S$): C 55.59 (55.80); H 7.96 (7.80); N none (0.00).

Synthesis of Disulfide $S_2P_2(C_6H_{10})_2$ (1-S_2). A 1:1 toluene−THF solution (8 mL) of $SSbPh_3$ (321 mg, 0.83 mmol, 2.0 equiv) was added to a toluene (2 mL) solution of **1** (94 mg, 0.41 mmol, 1.0 equiv). After 5 min of vigorous stirring, a white precipitate started forming. After 2 h of stirring, Et_2O (5 mL) was added to precipitate all of the product. A white powder consisting of analytically pure $S_2P_2(C_6H_{10})_2$ (105 mg,

dx.doi.org/10.1021/ic401052a | Inorg. Chem. 2013, 52, 8851−8864

0.36 mmol, 87%) was collected by filtering on a fritted glass filter, washing with Et_2O (10 mL) and drying under reduced pressure. ^1H NMR ($CDCl_3$, 20 °C, 400 MHz) δ: 2.93 (br s, 8 H, CH_2), 1.87 (s, 12 H, CH_3) ppm. ^{13}C NMR ($CDCl_3$, 20 °C, 100.6 MHz) δ: 125.5 (s, CH_0), 38.8 (vt, $^{12}J_{CP}$ = 19.5 Hz, CH_2), 22.3 (s, CH_3) ppm. $^{31}P\{^1H\}$ NMR (C_6D_6, 20 °C, 121.5 MHz) δ: +20.4 (s) ppm. $^{31}P\{^1H\}$ NMR ($CDCl_3$, 20 °C, 162 MHz) δ: +22.1 (s) ppm. Elemental analysis [%] found (and calcd. for $C_{12}H_{20}P_2S_2$): C 49.59 (49.64); H 6.96 (6.94); N none (0.00).

Synthesis of Diiminodiphosphorane $(MesN)_2P_2(C_6H_{10})_2$ (1-$(NMes)_2$, nppn). A toluene (5 mL) solution of $MesN_3$ (1.416 g, 8.78 mmol, 2.0 equiv) was added dropwise to a stirring toluene (5 mL) solution of **1** (0.993 g, 4.39 mmol, 1.0 equiv) inside a 50 mL Schlenk flask. The reaction mixture was allowed to stir for 15 min to allow N_2 evolution before sealing the flask containing the mixture and bringing it outside of the glovebox. The flask was then connected to a reflux condenser and N_2 bubbler, and the mixture was heated to reflux overnight. After cooling, the mixture was brought back into the glovebox, and concentrated by 50%. Et_2O (5 mL) and hexane (10 mL) were added to further precipitate the product, which was collected on a fritted glass filter, washed with hexane (30 mL), and dried under reduced pressure. The white crystalline solids consisting of analytically pure **1**-$(MesN)_2$ were collected (1.946 g, 3.85 mmol, 90% yield). Concentrating the filtrate and collecting the resulting solids yielded an additional amount of product (28 mg, 91% total yield). ^1H NMR ($CDCl_3$, 20 °C, 400.1 MHz) δ: 6.89 (s, 4 H, *m*-Mes), 2.65 (br dd, $^2J_{HH}$ = 14 Hz, 4 H, C*H*H), 2.38 (s, 12 H, *o*-Mes), 2.29 (s, 6 H, *p*-Mes), 2.08 (br d, 4 H, CH*H*), 1.39 (s, 12 H, CH_3) ppm. $^{13}C\{^1H\}$ NMR (C_6D_6, 20 °C, 100.6 MHz) δ: 131.7 (vt, J_{CP} = 6.5 Hz, *i*-Mes), 129.1 (*m*-Mes), 129.0 (*o*-Mes), 127.8 (*p*-Mes), 124.8 (*C*=*C*), 38.4 (vtr, J_{CP} = 29 Hz, CH_2), 21.6 (*o*-Mes), 21.4 (*p*-Mes), 21.3 (H_3C-C=C) ppm. $^{31}P\{^1H\}$ NMR (C_6D_6, 20 °C, 121.5 MHz) δ: −35.7 (s) ppm. Elemental analysis [%] found (and calcd. for $C_{30}H_{42}P_2N_2$): C 73.06 (73.14); H 8.46 (8.59); N 5.60 (5.69); P 12.70 (12.58). Allowing the crystals to age in air for 45 days at room temperature led to less than 10% decomposition (as assayed by ^1H NMR spectroscopy).

Synthesis of Molybdenum(II) Complex (nppn)MoCl(CO)$_2$(η^3-C_3H_5) (2). A dichloromethane solution (5 mL) of diiminodiphosphorane **1**-$(NMes)_2$ (84 mg, 0.17 mmol, 1.0 equiv) was added to a dichloromethane solution (5 mL) of $MoCl(CO)_2(\eta^3\text{-}C_3H_5)(MeCN)_2$ (53 mg, 0.17 mmol, 1.0 equiv). After 30 min of stirring, a bright yellow solid had started precipitating from the solution. After another 30 min, the mixture was layered with pentane (2 mL) and stored at −35 °C overnight to yield bright yellow solids, which were collected on a fritted glass filter. After washing with Et_2O (10 mL) and drying under reduced pressure, pale yellow solids were isolated consisting of analytically pure (nppn)$MoCl(CO)_2(\eta^3\text{-}C_3H_5)$ complex (112 mg, 0.155 mmol, 91% yield). ^1H NMR ($CDCl_3$, 20 °C, 400.1 MHz) δ: 6.99 (br s, 4 H, *m*-Mes), 4.83 (t, 2 H, CHH^{allyl}), 3.64 (m, 1 H, CH^{allyl}), 2.69 (dd, 2 H, PCH*H*), 2.8−2.4 (vbrs, 14 H, *o*-Mes, PC*H*H), 2.31 (s, 6 H, *p*-Mes), 2.06 (d, 2 H, PCH*H*), 1.77 (s, 6 H, CH_3), 1.66 (s, 6 H, CH_3), 0.62 (br s, 2 H, CHH^{allyl}) ppm. $^{13}C\{^1H\}$ NMR ($CDCl_3$, 20 °C, 125.8 MHz) δ: 227.8 (*C*O), 135−137 (vbr, *o*-Mes), 133.6 (*i*-Mes), 129.9 (*m*-Mes), 129.8 (*o*-Mes), 127.3 (*p*-Mes), 122.8 (*C*=*C*), 73.5 (CH^{allyl}), ∼63 (vbr, CH_2^{allyl}), 29.3 (br d, CH_2P), 24.3 (br, *o*-CH_3), 23.2 (*o*-CH_3), 21.0 (*p*-CH_3), 20.7 (br, H_3CC=CCH_3), 20.0 (H_3CC=CCH_3) ppm. $^{31}P\{^1H\}$ NMR ($CDCl_3$, 20 °C, 162.0 MHz) δ: +7.1 (br d, ^1J = 180 Hz), +5.6 (br d) ppm. Elemental analysis [%] found (and calcd. for $MoC_{35}H_{47}ClP_2N_2O_2$): C 57.33 (58.29); H 6.03 (6.57); N 3.62 (3.88).

Synthesis of Nickel(II) Complex (nppn)$NiCl_2$ (3). A suspension of diiminodiphosphorane **1**-$(NMes)_2$ (79 mg, 0.16 mmol, 1.0 equiv) in dichloromethane (5 mL) was added to a yellow suspension of $NiCl_2$(dme) (35 mg, 0.16 mmol, 1.0 equiv) in dichloromethane (5 mL). After 15 min, the color had changed slowly from yellow to an intense turquoise color. After 1 h of stirring, the solution was filtered though a glass paper plug to yield a deep blue filtrate and yellow solids. The filtrate was concentrated under reduced pressure (to ca. 1 mL) and then diluted with Et_2O (10 mL). The resulting blue solids were collected on a fritted glass filter, washed with Et_2O (5 mL), and dried to yield turquoise solids consisting of pure paramagnetic complex (nppn)$NiCl_2$ (77 mg, 0.12 mmol, 76% yield). ^1H NMR ($CDCl_3$, 20 °C, 400.1 MHz) δ: 42.5 (s, 6 H, *p*-Mes), 28.5 (br s, 12 H, *o*-Mes), 25.4 (s, 4 H, C*H*H), 22.5 (s, 4 H, CH*H*), 5.83 (br s, 4 H, *m*-Mes), 0.39 (s, 12 H, CH_3) ppm. Elemental analysis [%] found (and calcd. for $NiCl_2C_{30}H_{42}P_2N_2$): C 58.23 (57.91); H 6.86 (6.80); N 4.64 (4.50).

Synthesis of Nickel(II) Complex [(nppn)Ni(η^3-2-C_3H_4Me)]-[OTf] (4). A solution of diiminodiphosphorane (98 mg, 0.20 mmol, 1.0 equiv) in dichloromethane (5 mL) was added to a red suspension of $[NiCl(2\text{-}C_3H_4Me)]_2$ (30 mg, 0.10 mmol, 0.5 equiv) in dichloromethane (2 mL). AgOTf (51 mg, 0.20 mmol, 1.0 equiv) was added to this mixture as a slurry in dichloromethane (5 mL) leading to a color change from red to yellow-brown. After stirring for 1 h, the mixture was filtered though a pad of Celite (to remove the AgCl byproduct), and the solids were washed with dichloromethane until a colorless filtrate was obtained. The yellow filtrate was concentrated (to 5 mL), then pentane (1 mL) and diethyl ether (5 mL) were added. The resulting mixture was stirred for 1 min after which the golden solids were collected on a fritted glass filter and dried under reduced pressure to yield pure [(nppn)Ni(η^3-2-C_3H_4Me)][OTf] complex (89 mg, 0.12 mmol, 59% yield). ^1H NMR ($CDCl_3$, 20 °C, 400.1 MHz) δ: 6.87 (s, 2 H, *m*-Mes), 6.85 (s, 2 H, *m*-Mes), 3.44 (d, $^2J_{HH}$ = 16 Hz, 2 H, PCH*H*), 3.27 (d, 2 H, PCH*H*), 2.86 (s, 4 H, PC*H*H), 2.66 (s, 6 H, *o*-Mes), 2.40 (s, 6 H, *o*-Mes), 2.24 (s, 6 H, *p*-Mes), 2.13 (s, 3 H, CH_3^{allyl}), 1.86 (s, 6 H, CH_3), 1.81 (s, 6 H, CH_3), 1.59 (s, 2 H, CH_2^{allyl}), 1.39 (s, 2 H, CH_2^{allyl}) ppm. ^1H NMR (C_6D_6, 20 °C, 500 MHz) δ: 6.86 (s, 2 H, *m*-Mes), 6.84 (s, 2 H, *m*-Mes), 3.26 (d, 16 Hz, 2 H, CH_2), 2.86 (d, 2 H, CH_2), 2.69 (s, 6 H, *o*-Mes), 2.44 (m, 4 H, CH_2), 2.43 (s, 6 H, *o*-Mes), 2.19 (s, 6 H, *p*-Mes), 1.98 (s, 3 H, CH_3^{allyl}), 1.75 (s, 1 H, CH_2^{allyl}), 1.55 (s, 12 H, CH_3), 1.41 (s, 1 H, CH_2^{allyl}). ppm $^{13}C\{^1H\}$ NMR (C_6D_6, 20 °C, 125.8 MHz) δ: 141.8 (*i*-Mes), 135.0 (*o*-Mes), 133.8 (*o*-Mes), 133.4 (*p*-Mes), 129.8(*m*-Mes), 129.6 (*m*-Mes), 124.7 (*C*=*C*), 123.8 (CF_3), ∼83 (vbr, CH_0^{allyl}), 54.8 (CH_2^{allyl}), 32.9 (br d, J_{CP} = 18 Hz, CH_2), 22.9 (*o*-CH_3), 22.8 (CH_3^{allyl}), 22.7 (*o*-CH_3), 20.8 (H_3CC=CCH_3), 20.7(*p*-CH_3), 20.5 (H_3CC=CCH_3) ppm. $^{31}P\{^1H\}$ NMR ($CDCl_3$, 20 °C, 162.0 MHz) δ: +25.2 (s) ppm. ^{19}F NMR ($CDCl_3$, 20 °C, 282.4 MHz) δ: −78.6 (s) ppm. Elemental analysis [%] found (and calcd. for $NiC_{35}H_{49}P_2SN_2O_3F_3$): C 55.19 (55.64); H 5.91 (6.54); N 3.61 (3.71).

Calorimetric Measurements. In the glovebox, a solution of 0.0808 g of **1** (0.36 mmol) was dissolved in 6 mL of C_6D_6, and 1 mL of this stock solution was loaded into an NMR tube. The remaining 5 mL of solution were loaded into the Calvet calorimeter cell with MesCNO (0.0189 g, 0.1172 mmol) as limiting reagent. The calorimeter cell was sealed, taken from the glovebox, and loaded into the Setaram C-80 calorimeter. Following temperature equilibration, the reaction was initiated and the calorimeter rotated to achieve mixing. Following return to baseline the calorimeter cell was taken into the glovebox, opened, and 1 mL of the solution loaded into an NMR tube. ^{31}P NMR spectra of both the stock solution and the calorimetry solution were then acquired, and the reaction was confirmed as quantitative. The sole product was **1**-O and no detectable amount of **1**-O_2 was detected. The enthalpy of three measurements done in this way led to ΔH = −78.1 ± 1.9 kcal/mol based on the reaction

$$\mathbf{1}(\text{tol. sol.}) + \text{MesCNO(solid)} \xrightarrow{\Delta H} \mathbf{1}\text{-O(tol. sol.)} + \text{MesCN(tol. sol.)} \quad (6)$$

To these data the enthalpy of solution of MesCNO in toluene (+4.3 ± 0.1 kcal/mol) was subtracted to give ΔH_{rxn} = −82.4 ± 2.0 kcal/mol with all species in toluene solution. Because of the long reaction time of the second OAT reaction coupled with the low solubility of the product, the enthalpy of formation of **1**-O_2 could not be measured.

Reactions of $SSbPh_3$ and **1** were performed in a similar manner. In contrast to reaction with MesCNO which showed with limiting MesCNO that only the monosubstituted product was formed, even with $SSbPh_3$ as limiting reagent small but detectable levels of the disubstituted product **1**-S_2 were identified. The average value for the first substitution (which included traces of disubstituted product) was −20.4 ± 0.5 kcal/mol. Because of its apparently greater solubility in

dx.doi.org/10.1021/ic401052a | Inorg. Chem. 2013, 52, 8851−8864

Table 4. Crystallographic Data for Diphosphane Oxides 1-O, 1-O_2, and 1-O_3

	1-O	1-O_2	1-O_3
reciprocal net code/CCDC no.	D8_11005/898603	D8_11006/898604	X8_10087/898605
empirical formula, FW (g/mol)	$C_{12}H_{20}OP_2$, 242.22	$C_{12}H_{20}O_2P_2$, 258.22	$C_{12}H_{20}O_3P_2$, 274.22
crystal size (mm^3)	0.40 × 0.30 × 0.20	0.30 × 0.20 × 0.10	0.12 × 0.10 × 0.05
temperature (K)	100(2)	100(2)	100(2)
wavelength (A)	1.54178	1.54178	0.71073
crystal system, space group	monoclinic, $P2_1/c$	orthorhombic, $Pnma$	trigonal, $P\bar{1}$
unit cell dimensions (Å, deg)	a = 10.8769(2), α = 90	a = 9.59800(10), α = 90	a = 7.6898(6), α = 93.956(2)
	b = 6.92120(10), β = 104.9620(10)	b = 20.1851(3), β = 90	b = 8.1011(6), β = 98.939(2)
	c = 17.2230(3), γ = 90	c = 6.58950(10), γ = 90	c = 10.7689(8), γ = 101.833(2)
volume (A^3)	1252.61(4)	1276.63(3)	645.09(8)
Z	4	4	2
density (calc, g/cm^3)	1.284	1.343	1.412
absorption coefficient (mm^{-1})	2.924	2.964	0.331
$F(000)$	520	552	292
θ range for data collection (deg)	4.21 to 69.82	4.38 to 69.89	1.92 to 30.51
index ranges	$-13 \le h \le 13$,	$-11 \le h \le 11$,	$-10 \le h \le 10$,
	$-8 \le k \le 7$,	$-23 \le k \le 24$,	$-11 \le k \le 11$,
	$-20 \le l \le 20$	$-5 \le l \le 7$	$-15 \le l \le 15$
reflections collected	24434	11533	42402
independent reflections, R_{int}	2375 (0.0259)	1229 (0.0269)	3904 (0.0503)
completeness to θ_{max} (%)	99.6	99.0	98.9
max. and min transmission	0.5924 and 0.3876	0.7559 and 0.4700	0.9836 and 0.9613
data/restraints/parameters	2375/0/140	1229/0/81	3904/33/183
goodness-of-fit[a]	1.086	1.077	1.171
final R indices[b] [$I > 2\sigma(I)$]	R_1 = 0.0293,	R_1 =0.0291,	R_1 =0.0531,
	wR_2 = 0.0757	wR_2 = 0.0815	wR_2 = 0.1453
R indices[b] (all data)	R_1 = 0.0293,	R_1 = 0.0302,	R_1 =0.0599,
	wR_2 = 0.0757	wR_2 = 0.0823	wR_2 = 0.1502
largest diff. peak and hole ($e \cdot Å^{-3}$)	0.287 and −0.276	0.359 and −0.269	0.816 and −0.779

[a] $\mathrm{GoF} = [(\sum[w(F_o^2 - F_c^2)^2])/(n-p)]^{1/2}$. [b] $R_1 = (\sum||F_o| - |F_c||)/(\sum|F_o|)$; $wR_2 = [(\sum[w(F_o^2 - F_c^2)^2)/(\sum[w(F_o^2)^2])]^{1/2}$; $w = (1)/(\sigma^2(F_o^2) + (aP)^2 + bP)$; $P = (2F_c^2 + \max(F_o^2, 0))/(3)$.

toluene, the enthalpy of conversion of **1**-S to **1**-S_2 could be measured and was found to be −21.7 ± 0.6 kcal/mol. The difference in enthalpies of substitution 1.3 ± 1.0 kcal/mol showed the second enthalpy of sulfurization to be slightly more exothermic than the first. Because of this small difference, no correction for the small amount of disubstituted product detected in the first sulfurization was needed. To evaluate the bond strengths in solution, the enthalpy of solution of $SSbPh_3$ in toluene (+5.3 ± 0.5 kcal/mol) must be subtracted giving final enthalpies of sulfurization of −25.7 ± 1.0 kcal/mol for formation of **1**-S from **1** and −27.0 ± 1.1 kcal/mol for formation of **1**-S_2 from **1**-S.

Computational Details. Electronic structure calculations for thermodynamic values were carried out using the M05-2X[42] density functional with the 6-311G(3df,2p) basis set as implemented in the Gaussian 09 suite of programs.[43] Minimum energy and transition state structures were optimized by computing analytical energy gradients. The obtained stationary points were characterized by performing energy second derivatives, confirming them as minima or first order saddle points by the number of negative eigenvalues of the Hessian matrix of the energy (zero and one negative eigenvalues respectively). Computed electronic energies were corrected for zero-point energy and thermal energy to obtain the corresponding thermodynamic property H^0. To derive binding energies, the basis set superposition error (BSSE) was computed using counterpoise calculations.[44] All structures were derived from the reported crystal structures of **1** and **1**-O_2 after truncating the CH_3 groups to H.

Intrinsic reaction coordinate (IRC)[45] calculations were done to describe the reaction mechanisms for 2,6-$Me_2C_6H_3CNO$ and PhCNO with **1**′ and **1**′-O, providing the connection between the minimum energy points through the different transitions states. Further optimization of the final points of the IRCs was done to obtain the real minimum energy structures. Neither minima nor transition states could be located corresponding to a 1,3-cycloaddition of 2,6-$Me_2C_6H_3CNO$ to the diphosphane **1**′ via a concerted mechanism. Likewise, direct OAT from RCNO to the diphosphane was found to be repulsive and did not lead to reaction. No transition states were found to contain a 5-membered {P_2ONC} ring presumably because of the repulsion between the lone pair electrons of the O atom and the unactivated P atom. The second OAT does not involve a transition state containing a six-membered {POCNOP} cycle with the nitrile-oxide C and O atoms binding to the oxo atom and the other P atom of the substrate, presumably because of the repulsion between the lone pair electrons of the second P atom and the O atom of the nitrile oxide.

Using a value of 52.3 kcal/mol for the N−O BDE in MesCNO,[28] and 94 kcal/mol for the P−S BDE in $SPMe_3$,[32] the computed reaction enthalpies below yielded the following E−P BDEs:

$$\mathbf{1} + \mathrm{MesCNO} \xrightarrow{\Delta H = -78.7\ \mathrm{kcal/mol}} \mathbf{1}\text{-O} + \mathrm{MesCN} \Rightarrow$$
$$\text{P−O in } \mathbf{1}\text{-O: } 131.1\ \mathrm{kcal/mol} \quad (7)$$

$$\mathbf{1}\text{-O} + \mathrm{MesCNO} \xrightarrow{\Delta H = -72.5\ \mathrm{kcal/mol}} \mathbf{1}\text{-}O_2 + \mathrm{MesCN} \Rightarrow$$
$$\text{P−O in } \mathbf{1}\text{-}O_2\text{: } 124.8\ \mathrm{kcal/mol} \quad (8)$$

$$\mathbf{1} + \mathrm{SPMe_3} \xrightarrow{\Delta H = +3.7\ \mathrm{kcal/mol}} \mathbf{1}\text{-S} + \mathrm{PMe_3} \Rightarrow$$
$$\text{P−S in } \mathbf{1}\text{-S: } 90\ \mathrm{kcal/mol} \quad (9)$$

$$\mathbf{1}\text{-S} + \mathrm{SPMe_3} \xrightarrow{\Delta H = +8.9\ \mathrm{kcal/mol}} \mathbf{1}\text{-}S_2 + \mathrm{PMe_3} \Rightarrow$$
$$\text{P−S in } \mathbf{1}\text{-}S_2\text{: } 85\ \mathrm{kcal/mol} \quad (10)$$

dx.doi.org/10.1021/ic401052a | Inorg. Chem. 2013, 52, 8851−8864

Table 5. Crystallographic Data for Disulfide 1-S_2 and Diiminodiphosphoranes 1-$(NMes)_2$ and 1-$(NCPh_3)(NMes)$

	1-S_2	1-$(NMes)_2$	1-$(NCPh_3)(NMes)$
reciprocal net code/CCDC no.	11224/898606	D8_11049/898607	X8_11203/898608
empirical formula, FW (g/mol)	$C_{12}H_{20}P_2S_2$, 290.34	$C_{30}H_{42}N_2P_2$, 492.60	$C_{40}H_{46}N_2P_2$, 616.73
crystal size (mm^3)	0.30 × 0.10 × 0.06	0.35 × 0.12 × 0.10	0.30 × 0.05 × 0.05
temperature (K)	100(2)	100(2)	100(2)
wavelength (Å)	0.71073	1.54178	0.71073
crystal system, space group	monoclinic, $P2_1/c$	monoclinic, $P2_1/c$	monoclinic, $P2_1/c$
unit cell dimensions (Å, deg)	a = 6.7523(6), α = 90	a = 12.43340(10), α = 90	a = 18.026(2), α = 90
	b = 18.5199(17), β = 90.3740(10)	b = 15.8501(2), β = 98.4980(10)	b = 9.1399(11), β = 102.766(3)
	c = 11.2782(11), γ = 90	c = 13.8650(2), γ = 90	c = 20.939(3), γ = 90
volume ($Å^3$)	1410.3(2)	2702.39(6)	3364.5(7)
Z	4	4	4
density (calc, g/cm^3)	1.367	1.211	1.218
absorption coefficient (mm^{-1})	0.577	1.603	0.160
$F(000)$	616	1064	1320
θ range for data collection (deg)	2.11 to 30.50	3.59 to 69.66	1.16 to 27.88
index ranges	$-9 \le h \le 9$,	$-15 \le h \le 15$,	$-23 \le h \le 23$,
	$-26 \le k \le 26$,	$-19 \le k \le 19$,	$-12 \le k \le 10$,
	$-16 \le l \le 16$	$-11 \le l \le 15$	$-27 \le l \le 27$
reflections collected	38978	55585	103303
independent reflections, R_{int}	4311 (0.0383)	4971 (0.0403)	8011 (0.0793)
completeness to θ_{max} (%)	100.0	97.6	100.0
max. and min transmission	0.9662 and 0.8459	0.8561 and 0.6038	0.9920 and 0.9535
data/restraints/parameters	4311/0/149	4971/0/317	8011/0/404
goodness-of-fit[a]	1.057	1.032	1.078
final R indices[b] [$I > 2\sigma(I)$]	R_1 = 0.0227,	R_1 = 0.0372,	R_1 =0.0446,
	wR_2 = 0.0589	wR_2 = 0.0990	wR_2 = 0.1100
R indices[b] (all data)	R_1 =0.0272, wR_2 = 0.0619	R_1 =0.0448, wR_2 = 0.1052	R_1 =0.0627, wR_2 = 0.1196
largest diff. peak and hole ($e·Å^{-3}$)	0.466 and −0.270	0.370 and −0.325	0.527 and −0.317

[a] GoF = $[\sum([w(F_o^2 - F_c^2)^2])/((n-p))]^{1/2}$. [b] $R_1 = (\sum||F_o| - |F_c||)/(\sum|F_o|)$; $wR_2 = [(\sum[w(F_o^2 - F_c^2)^2)/(\sum[w(F_o^2)^2])]^{1/2}$; $w = (1)/(\sigma^2(F_o^2) + (aP)^2 + bP)$; $P = (2F_c^2 + \max(F_o^2, 0))/(3)$.

All the other computations were carried out using the ORCA 2.9 quantum chemistry program package from the development team at the University of Bonn.[46] The LDA functional employed was that of Perdew (PW-LDA)[47] while the GGA part was handled using the functionals of Becke and Perdew (BP86).[48] In addition, all calculations were carried out using the Zero-Order Regular Approximation (ZORA),[49] in conjunction with the SARC-TZV basis set hydrogen, SARC-TZV(2pf) set for metals, and SARC-TZV(p) set for all other atoms.[50] Spin-restricted Kohn−Sham determinants have been chosen to describe the closed-shell wave functions, employing the RI approximation and the tight SCF convergence criteria provided by ORCA. The structures were derived from the reported crystal structure of 1-$(NMes)_2$ by removing one imine group, and replacing the other as necessary. The CO stretching frequencies were obtained by constructing a $Ni(CO)_3$ fragment on the free phosphorus atom in MOLDEN[51] For the open-shell wave functions of $[1]^{\bullet+}$ and $[1\text{-O}]^{\bullet+}$ the B3LYP functional, 6-31G basis set, spin-unrestricted Kohn−Sham determinants were used. The optimized structures were rendered using PLATON[52] while the NBO distributions were computed using GENNBO.[53] The coordinates for all optimized structures are provided in the Supporting Information.

X-ray Crystallographic Details. Diffraction quality crystals were obtained typically from saturated, hot solutions by allowing them to slowly cool down to room temperature. Colorless crystals of 1-O, 1-$(NMes)(NCPh_3)$, and 1-$(NMes)_2$ were obtained from hot benzene; colorless crystals of 1-S_2 and turquoise crystals of **3** from hot THF; colorless crystals of 1-O_2 from hot DMSO. Yellow crystals of **2** were grown from a chloroform solution which was allowed to slowly evaporate at room temperature. A colorless crystal of 1-O_3 was obtained by allowing a benzene solution of diphosphane **1** to age in an NMR tube capped with a plastic cap. Low-temperature (100 K) data were collected on a Siemens Platform three-circle diffractometer coupled to a Bruker-AXS Smart Apex CCD detector with graphite-monochromated Mo Kα radiation (λ = 0.71073 Å) for the structure of disulfide 1-S_2 and complex **3**; on a Bruker-AXS X8 Kappa Duo diffractometer coupled to a Smart Apex2 CCD detector with Mo Kα radiation (λ = 0.71073 Å) for the structure of the trioxide 1-O_3, the diiminodiphosphorane 1-$(NMes)(NCPh_3)$, and complex **2**; on a Bruker D8 three-circle diffractometer coupled to a Bruker-AXS Smart Apex CCD detector with graphite-monochromated Cu Kα radiation (λ = 1.54178 Å) for the structures of the oxides 1-O and 1-O_2, and the complex **3** (φ- and ω-scans). General refinement details have been described elsewhere.[4,54] Reported structures were rendered using PLATON.[52] Specific details are provided in the text and tables below, and in the form of .cif files available from the CCDC.[55]

The monoxide 1-O, disulfide 1-S_2, and diiminodiphosphoranes 1-$(NMes)(NCPh_3)$ and 1-$(NMes)_2$ crystallized in the monoclinic space group $P2_1/c$, each with one molecule of the *exo-endo* conformer per asymmetric unit (Tables 4 and 5). The dioxide 1-O_2 crystallized in the orthorhombic space group *Pnma*, with half of a molecule of the *exo-exo* conformer per asymmetric unit, and a symmetry plane containing the phosphorus and oxygen atoms. All these models contain no solvent, no disorder, and no restraints.

The trioxide 1-O_3 co-crystallized with an isomer of the dioxide 1-O_2 in the triclinic space group $P\bar{1}$, with one molecule of *exo-endo* conformer per asymmetric unit. Only the central part consisting of one P atom and the O atoms is disordered between the trioxide and the dioxide, while the remaining atoms overlap between the two constituents. The hydrogen atoms of the CH_2 groups adjacent to the disordered P atom were each refined over two positions. Similarity restraints on 1−2 and 1−3 distances and displacement parameters as well as rigid bond restraints for anisotropic displacement parameters were applied to the phosphorus and oxygen atoms. The ratio between

dx.doi.org/10.1021/ic401052a | Inorg. Chem. 2013, 52, 8851−8864

Table 6. Crystallographic Data for Molybdenum Complex 2 and Nickel Complex 3

	2	3
reciprocal net code/CCDC no.	X8_12025/898609	11228/898610
empirical formula, FW (g/mol)	$C_{35}H_{47}ClMoN_2O_2P_2\cdot 3CHCl_3$, 1079.18	$C_{30}H_{42}Cl_2N_2NiP_2\cdot 2C_4H_80$, 766.41
color/morphology	yellow/block	blue/block
crystal size (mm^3)	0.10 × 0.10 × 0.05	0.30 × 0.20 × 0.10
temperature (K)	100(2)	100(2)
wavelength (Å)	0.71073	0.71073
crystal system, space group	monoclinic, $P2_1/n$	orthorhombic, $P2_12_12_1$
unit cell dimensions (Å, deg)	a = 13.838(2), α = 90	a = 9.5206(7), α = 90
	b = 18.902(3), β = 110.417(3)	b = 16.9847(14), β = 90
	c = 19.269(3), γ = 90	c = 23.9758(19), γ = 90
volume ($Å^3$)	4723.6(14)	3877.0(5)
Z	4	4
density (calc, g/cm^3)	1.517	1.313
absorption coefficient (mm^{-1})	0.946	0.756
F(000)	2200	1632
θ range for data collection (deg)	1.56 to 29.13	1.47 to 28.28
index ranges	$-18 \le h \le 18$,	$-12 \le h \le 12$,
	$-25 \le k \le 25$,	$-22 \le k \le 22$,
	$-26 \le l \le 26$	$-31 \le l \le 31$
reflections collected	111074	93247
independent reflections, R_{int}	12696(0.0605)	9623 (0.0709)
completeness to θ_{max} (%)	100.0	100.0
max. and min transmission	0.9542 and 0.9113	0.9283 and 0.8051
data/restraints/parameters	12696/119/613	9623/434/520
goodness-of-fit[a]	1.141	1.073
final R indices[b] [$I > 2\sigma(I)$]	R_1 =0.0431,	R_1 = 0.0453,
	wR_2 = 0.0832	wR_2 = 0.1081
R indices[b] (all data)	R_1 = 0.0566,	R_1 = 0.0591,
	wR_2 = 0.0879	wR_2 = 0.1180
largest diff. peak and hole ($e\cdot Å^{-3}$)	0.928 and −0.789	0.705 and −0.518

[a] GooF = $[\sum([w(F_o^2 - F_c^2)^2])/((n-p))]^{1/2}$. [b] $R_1 = (\sum||F_o| - |F_c||)/(\sum|F_o|)$; $wR_2 = [(\sum[w(F_o^2 - F_c^2)^2)/(\sum[w(F_o^2)^2])]^{1/2}$; $w = (1)/(\sigma^2(F_o^2) + (aP)^2 + bP)$; $P = (2F_c^2 + \max(F_o^2, 0))/(3)$.

the two components of the disorder was refined freely, and the sum of the two occupancies for each pair was constrained to unity.

The molybdenum complex **2** crystallized in monoclinic space group $P2_1/n$ with one molecule of complex and three molecules of $CHCl_3$, while the nickel complex **3** crystallized in the orthorhombic space group $P2_12_12_1$ with one molecule of complex and two molecules of THF (Table 6). In both cases, the complexes contained no disorders, but all solvent molecules required modeling over two positions. The occupancy of each position was refined freely, and their sums were restrained to unity. Similarity restraints on 1−2 and 1−3 distances and displacement parameters, as well as rigid bond restraints for anisotropic displacement parameters were applied to the disordered fragments.

■ ASSOCIATED CONTENT

Ⓢ Supporting Information

Additional synthetic, spectroscopic, and computational details. This material is available free of charge via the Internet at http://pubs.acs.org.

■ AUTHOR INFORMATION

Corresponding Author

*E-mail: manuel.temprado@uah.es (M.T.), c.hoff@miami.edu (C.D.H.), ccummins@mit.edu (C.C.C.).

Notes

The authors declare no competing financial interest.

■ ACKNOWLEDGMENTS

This material is based upon work supported by the National Science Foundation under CHE-1111357 (C.C.C.) and CHE-0615743 (C.D.H.); and Spanish Ministry of Economy and Competitiveness (MINECO) under CTQ2012-36966 (M.T.). We thank Thermphos International for support including a gift of white phosphorus, Dr. Peter Müller and Dr. Michael Takase for assistance with crystallography, and Anthony Cozzolino for assistance with computations.

■ REFERENCES

(1) Piro, N. A.; Figueroa, J. S.; McKellar, J. T.; Cummins, C. C. *Science* **2006**, *313*, 1276−1279.

(2) Tofan, D.; Cummins, C. C. *Angew. Chem., Int. Ed.* **2010**, *49*, 7516−7518.

(3) 3,4,8,9-Tetramethyl-1,6-diphosphabicyclo[4.4.0]deca-3,8-diene may also be found under the CAS #1258870-28-8 or the alternative name 1,4,6,9-tetrahydro-2,3,7,8-tetramethyl-[1,2]diphosphorino[1,2-*a*][1,2]diphosphorin.

(4) Tofan, D.; Cummins, C. C. *Chem. Sci.* **2012**, *3*, 2474−2478.

(5) (a) Johnson, A. W. *Ylides and Imines of Phosphorus*; John Wiley, New York, 1993. (b) Collins, S. *Handbook of Transition Metal Polymerization Catalysts*; John Wiley & Sons, Inc., 2010; Chapter Ethylene Polymerization and α-Olefin Oligomerization Using Catalysts Derived from Phosphoranes and Ni(II) and Ni(0) Precursors, pp 459−466.

(6) Claver, C.; Gili, F.; Viñas, J.; Ruiz, A. *Polyhedron* **1987**, *6*, 1329−1335.

(7) Li, G. Y.; Marshall, W. J. *Organometallics* **2002**, *21*, 590−591.
(8) (a) Meek, D. W.; Nicpon, P. *J. Am. Chem. Soc.* **1965**, *87*, 4951−4952. (b) Ainscough, E. W.; Bergen, H. A.; Brodie, A. M.; Brown, K. A. *J. Chem. Soc., Dalton Trans.* **1976**, 1649−1656. (c) Schmutzler, R.; Halfpenny, M. T.; Levason, W.; McAuliffe, C. A. *J. Chem. Soc., Dalton Trans.* **1978**, 1662−1663. (d) McQuillan, G. P.; Oxton, I. A. *J. Chem. Soc., Dalton Trans.* **1979**, 895−900. (e) Pomeroy, R. K.; Wijesekera, K. S. *Can. J. Chem.* **1980**, *58*, 206−209. (f) Kuhn, N.; Winter, M. *J. Organomet. Chem.* **1982**, *239*, C31−C34. (g) Et, D. T.; Legros, J.-P. *Phosphorus Sulfur Relat. Elem.* **1983**, *14*, 377−380. (h) Troy, S.; Legros, J.-P.; McQuillan, G. *Inorg. Chim. Acta* **1983**, *72*, 119−126. (i) Subasi, E.; Sentürk, O. S. *Synth. React. Inorg., Met.-Org., Nano-Met. Chem.* **2011**, *41*, 834−838.
(9) (a) Almond, M. J.; Sarikahya, F.; Sentürk, O. S. *Polyhedron* **1997**, *16*, 1101−1103. (b) Sentürk, O. S.; Shekhel, H. A.; Sterenberg, B. T.; Udachin, K. A.; Sert, S.; Özdemir, U.; Sarikahya, F. U. *Polyhedron* **2003**, *22*, 1659−1664.
(10) (a) Hieber, W.; Kummer, R. *Z. Anorg. Allg. Chem.* **1966**, *344*, 292−305. (b) Roesky, H. W.; Djarrah, H.; Thomas, M.; Krebs, B.; Henkel, G. *Z. Naturforsch. B* **1983**, *38B*, 168−171.
(11) Westland, A. D.; Haque, F.; Bouchard, J. M. *Inorg. Chem.* **1980**, *19*, 2255−2259.
(12) Kuhn, N.; Winter, M. *J. Organomet. Chem.* **1983**, *246*, C80−C82.
(13) Cotton, F. A.; Frenz, B. A.; Hunter, D. L.; Mester, Z. C. *Inorg. Chim. Acta* **1974**, *11*, 111−117.
(14) (a) Liu, H.; Calhorda, M. J.; Drew, M. G.; Félix, V. *Inorg. Chim. Acta* **2003**, *347*, 175−180. (b) Claver, C.; Ruiz, A.; Masdeu, A. M.; Viñas, J.; Saballs, T.; Lahoz, F. J.; Plou, F. J. *J. Organomet. Chem.* **1989**, *373*, 269−278. (c) Legros, J.-P.; Troy, D. *Acta Crystallogr., Sect. B* **1983**, *39*, 337−343.
(15) Cotton, F. A.; Frenz, B. A.; Hunter, D. L.; Mester, Z. C. *Inorg. Chim. Acta* **1974**, *11*, 119−122.
(16) (a) Schmidt, U.; Boie, I. *Angew. Chem., Int. Ed.* **1966**, *5*, 1038−1038. (b) Schmidt, U.; Boie, I.; Osterroht, C.; Schröer, R.; Grützmacher, H.-F. *Chem. Ber.* **1968**, *101*, 1381−1397. (c) Kawashima, T.; Shimamura, M.; Inamoto, N. *Heterocycles* **1984**, *21*, 751. (d) Brieden, W.; Kellersohn, T. *Chem. Ber.* **1993**, *126*, 845−847.
(17) (a) Sheldrick, W. S.; Pohl, S.; Zamankhan, H.; Banek, M.; Amirzadeh-Asl, D.; Roesky, H. W. *Chem. Ber.* **1981**, *114*, 2132−2137. (b) Alder, R. W.; Ganter, C.; Gil, M.; Gleiter, R.; Harris, C. J.; Harris, S. E.; Lange, H.; Guy Orpen, A.; Taylor, P. N. *J. Chem. Soc., Perkin Trans. 1* **1998**, 1643−1656.
(18) Teramoto, Y.; Kubo, K.; Mizuta, T. *J. Organomet. Chem.* **2011**, *696*, 3402−3407.
(19) (a) Vrieze, K.; Koten, G. V. *Inorg. Chim. Acta* **1985**, *100*, 79−96. (b) Myeongsoon, K.; Ayusman, S.; Lev, Z.; L., R. A. *Beyond Metallocenes*; American Chemical Society: Washington, DC, 2003; Chapter 12, pp 143−153; (c) Klein, A.; Budnikova, Y. H.; Sinyashin, O. G. *J. Organomet. Chem.* **2007**, *692*, 3156−3166. (d) Ivanchev, S. S. *Russ. Chem. Rev.* **2007**, *76*, 617. (e) Anselment, T. M. J.; Vagin, S. I.; Rieger, B. *Dalton Trans.* **2008**, 4537−4548. (f) Guan, Z.; Popeney, C. S. In *Metal Catalysis in Olefin Polymerization*; Guan, Z., Ed.; Topics in Organometallic Chemistry; Springer-Verlag: London, U.K., 2009; Vol. *26*; Chapter Recent Progress in Late Transition Metal α-Diimine Catalysts for Olefin Polymerization, pp 179−220.
(20) Ittel, S. D.; Johnson, L. K.; Brookhart, M. *Chem. Rev.* **2000**, *100*, 1169−1204.
(21) (a) Link, M.; Niecke, E.; Nieger, M. *Chem. Ber.* **1994**, *127*, 313−319. (b) Lukashev, N. V.; Averin, A. D.; Zhichkin, P. E.; Kazankova, M. A.; Beletskaya, I. P. *Phosphorus Sulfur Relat. Elem.* **1996**, *109*, 609−612.
(22) Appel, R.; Milker, R. *Chem. Ber.* **1974**, *107*, 2658−2670.
(23) (a) Appel, R.; Milker, R.; Ruppert, I. *Z. Anorg. Allg. Chem.* **1977**, *429*, 69−73. (b) Appel, R.; Milker, R. *Chem. Ber.* **1977**, *110*, 3201−3204.
(24) (a) Arisawa, M.; Onoda, M.; Hori, C.; Yamaguchi, M. *Tetrahedron Lett.* **2006**, *47*, 5211−5213. (b) Kawaguchi, S.; Nagata, S.; Nomoto, A.; Sonoda, M.; Ogawa, A. *J. Org. Chem.* **2008**, *73*, 7928−7933.
(25) (a) Mackewitz, T. W.; Peters, C.; Bergsträsser, U.; Leininger, S.; Regitz, M. *J. Org. Chem.* **1997**, *62*, 7605−7613. (b) Keglevich, G.; Farkas, R.; Ludányi, K.; Kudar, V.; Hanusz, M.; Simon, K. *Heteroat. Chem.* **2005**, *16*, 104−110.
(26) Fave, C.; Hissler, M.; Kárpáti, T.; Rault-Berthelot, J.; Deborde, V.; Toupet, L.; Nyulázi, L.; Réau, R. *J. Am. Chem. Soc.* **2004**, *126*, 6058−6063.
(27) Glendening, E. D.; Landis, C. R.; Weinhold, F. *WIREs Comput. Mol. Sci.* **2012**, *2*, 1−42, DOI: 10.1002/wcms.51.
(28) Cai, X.; Majumdar, S.; Fortman, G. C.; Frutos, L. M.; Temprado, M.; Clough, C. R.; Cummins, C. C.; Germain, M. E.; Palluccio, T.; Rybak-Akimova, E. V.; Captain, B.; Hoff, C. D. *Inorg. Chem.* **2011**, *50*, 9620−9630.
(29) (a) Staudinger, H.; Meyer, J. *Helv. Chim. Acta* **1919**, *2*, 635−646. (b) Gololobov, Y. G.; Zhmurova, I. N.; Kasukhin, L. F. *Tetrahedron* **1981**, *37*, 437−472. (c) Bebbington, M. W.; Bourissou, D. *Coord. Chem. Rev.* **2009**, *253*, 1248−1261.
(30) Stewart, B.; Harriman, A.; Higham, L. J. *Organometallics* **2011**, *30*, 5338−5343.
(31) Faller, J. W. In *Comprehensive Organometallic Chemistry III*; Crabtree, R. H., Mingos, D. M. P., Eds.; Elsevier: Oxford, U.K., 2007; Vol. *1*: Fundamentals; pp 407−427.
(32) Capps, K. B.; Wixmerten, B.; Bauer, A.; Hoff, C. D. *Inorg. Chem.* **1998**, *37*, 2861−2864.
(33) Tolman, C. A. *Chem. Rev.* **1977**, *77*, 313−348.
(34) (a) Cavell, G. R.; Aparna, K.; Kamalesh Babu, P. R.; Wang, Y. Q. *J. Mol. Catal. A: Chem.* **2002**, *189*, 137−143. (b) Wei, R. P.; Stephan, W. D. *Organometallics* **2002**, *21*, 1308−1310. (c) Hill, S. M.; Hitchcock, B. P. *J. Chem. Soc., Dalton Trans.* **2002**, 4694−4702. (d) Gamer, T. M.; Rastatter, M.; Roesky, W. P.; Steffens, A.; Glanz, M. *Chem.—Eur. J.* **2005**, *11*, 3165−3172. (e) Rastatter, M.; Zulys, A.; Roesky, W. P. *Chem. Commun.* **2006**, 874−876. (f) Wiecko, M.; Roesky, W. P.; Burlakov, V. V.; Spannenberg, A. *Eur. J. Inorg. Chem.* **2007**, 876−881. (g) Gamer, T. M.; Roesky, W. P.; Palard, I.; Le Hellaye, M.; Guillaume, M. S. *Organometallics* **2007**, *26*, 651−657. (h) Klemps, C.; Buchard, A.; Houdard, R.; Auffrant, A.; Mezailles, N.; Le Goff, F. X.; Ricard, L.; Saussine, L.; Magna, L.; Le Floch, P. *New J. Chem.* **2009**, *33*, 1748−1752. (i) Buchard, A.; Platel, H. R.; Auffrant, A.; Le Goff, F. X.; Le Floch, P.; Williams, K. C. *Organometallics* **2010**, *29*, 2892−2900. (j) Jenter, J.; Roesky, W. P.; Ajellal, N.; Guillaume, M. S.; Susperregui, N.; Maron, L. *Chem.—Eur. J.* **2010**, *16*, 4629−4638.
(35) Alonso, J. C.; Neves, P.; Pires da Silva, M. J.; Quintal, S.; Vaz, P. D.; Silva, C.; Valente, A. A.; Ferreira, P.; Calhorda, M. J.; Félix, V.; Drew, M. G. B. *Organometallics* **2007**, *26*, 5548−5556.
(36) Clark, D. A.; Jones, D. L.; Mawby, R. J. *J. Chem. Soc., Dalton Trans.* **1980**, 565−569.
(37) Coe, B. J.; Glenwright, S. J. *Coord. Chem. Rev.* **2000**, *203*, 5−80.
(38) Fulmer, G. R.; Miller, A. J. M.; Sherden, N. H.; Gottlieb, H. E.; Nudelman, A.; Stoltz, B. M.; Bercaw, J. E.; Goldberg, K. I. *Organometallics* **2010**, *29*, 2176−2179.
(39) (a) Grundmann, C.; Dean, J. M. *J. Org. Chem.* **1965**, *30*, 2809−2812. (b) Barybin, M. V.; Diaconescu, P. L.; Cummins, C. C. *Inorg. Chem.* **2001**, *40*, 2892−2897.
(40) Ugi, I.; Perlinger, H.; Behringer, L. *Chem. Ber.* **1958**, *91*, 2330−2336.
(41) (a) Saunders, W. H.; Ware, J. C. *J. Am. Chem. Soc.* **1958**, *80*, 3328−3332. (b) Wiberg, N.; Neruda, B. *Chem. Ber.* **1966**, *99*, 740−749. (c) Thayer, J. S.; West, R. *Inorg. Chem.* **1964**, *3*, 406−409.
(42) Zhao, Y.; Schultz, N. E.; Truhlar, D. G. *J. Chem. Theory Comput.* **2006**, *2*, 364−382.
(43) Frisch, M. J. et al. *Gaussian 09*, Revision B.01; Gaussian, Inc.: Wallingford, CT, 2010.
(44) (a) Simon, S.; Duran, M.; Dannenberg, J. J. *J. Chem. Phys.* **1996**, *105*, 11024−11031. (b) Boys, S. F.; Bernardi, F. *Mol. Phys.* **1970**, *19*, 553−566.
(45) (a) Fukui, K. *Acc. Chem. Res.* **1981**, *14*, 363−368. (b) Hratchian, H. P.; Schlegel, H. B. *J. Chem. Theory Comput.* **2005**, *1*, 61−69.

(46) Neese, F. *ORCA-an ab initio, Density Functional and Semi-empirical program package*, Version 2.9; University of Bonn: Bonn, Germany, 2012.
(47) Perdew, J. P.; Wang, Y. *Phys. Rev. B: Condens. Matter Mater. Phys.* **1992**, *45*, 13244−13249.
(48) (a) Becke, A. D. *Phys. Rev. A* **1988**, *38*, 3098−3100. (b) Perdew, J. P. *Phys. Rev. B Condens. Matter* **1986**, *33*, 8822−8824.
(49) (a) Lenthe, E.; Baerends, E. J.; Snijders, J. G. *J. Chem. Phys.* **1993**, *99*, 4597−4610. (b) Heully, J. L.; Lindgren, I.; Lindroth, E.; Lundqvist, S.; Maartensson-Pendrill, A. M. *J. Phys. B: At. Mol. Phys.* **1986**, *19*, 2799−2815.
(50) Schaefer, A.; Horn, H.; Ahlrichs, R. *J. Chem. Phys.* **1992**, *97*, 2571−2577.
(51) Schaftenaar, G. *MOLDEN-a pre- and post processing program of molecular and electronic structure*, Version 5.0; Centre for Molecular and Biomolecular Informatics: Nijmegen, The Netherlands, 2010.
(52) Spek, A. L. *Acta Crystallogr.* **2009**, *D65*, 148−155.
(53) Weinhold, F. *GENNBO, Natural Bond Orbital (NBO)*, 5.0 package.
(54) Tofan, D.; Cossairt, B. M.; Cummins, C. C. *Inorg. Chem.* **2011**, *50*, 12349−12358.
(55) These data can be obtained free of charge from The Cambridge Crystallographic Data Centre via http://www.ccdc.cam.ac.uk/data_request/cif.